Response to Anonymous Referee #2

We thank Anonymous Referee #2 for the evaluation and recommendations, which helped to improve the manuscript. In the following, a point-by-point reply is given, with the Referee comments in italic. Page and line numbers in the replies refer to the marked-up version of the manuscript.

1. <u>P1, L35</u>, *you may add something like "due to higher measurement signal to noise ratio" to explain it.*

Thank you. The sentence now is: We find that SCD uncertainties are smallest for high top-of-atmosphere reflectance levels with high measurement signal to noise ratios (P1, L34).

2. <u>P5, L10</u>, *suggest changing the sentence "...is such that...is possible" to "...makes...possible..." to make it more readable.*

We would like to keep the original expression because we feel it stresses the "cause-effect" type of relationship between the signal-to-noise ratio levels and achieving a spectral fit (P5 L14).

3. <u>P6, L6,</u> *suggest changing "achromatic" to "wavelength independent" to make it easier to understand.*

"Achromatic" is now replaced by "wavelength independent" (P6 L11).

4. **<u>P7, L1</u>**, *you may add something like "improvement of cloud retrievals using measurements in O2 bands" before ", Additionally" as this is one of the main advantages.*

This is a good remark, but we believe it does not fit in the section about the instrument and the quality of level-1 data.

<u>5. P8, L13-14</u>, *it was mentioned that high-pass filter is applied. But it is not reflected in equations (1) and (2), probably omitted? Please also clarify if the high-pass filter is applied to the trace gas cross sections.*

The polynomials P(λ) in Eq. (1) and P*(λ) in Eq. (2) effectively act as high-pass filter (added in Line 31 P11). For the intensity fit, absolute cross sections are used. For the optical density fit, differential cross sections are used. They result from subtracting *a* polynomial (*not the* DOAS fit polynomial, P*(λ)) from the absolute cross sections.

<u>6. In Tables 2 and 3</u>, *it might be useful to add the reference used in the fitting, e.g., average irradiance, monthly average irradiance, daily Earthshine radiance.*

For Table 2: Done (see P10; footnotes); For OMNO2A v1&v2 and OMINO2-QA4ECV the reference spectrum is the 2005-mean solar irradiance spectrum. For OMINO2-NASA, monthly averaged solar irradiance spectrum is used as reference. Lastly, for GONO2A-BIRA and GONO2A-QA4ECV daily solar irradiance spectrum is used as reference.

For Table 3: The reference spectrum used in each spectral fitting algorithm is already mentioned as footnote in Table 3 (P13).

7. P12, L20-25, *although Sun et al. (2017) shows that the slit function is stable over time, it also shows that derived in-flight slit functions are quite different from pre-launch slit functions especially in terms of cross-track dependence. Has the use of derived slit functions prior to the fit been tested as implemented in the GOME2 algorithms used in this study?*

We have done limited tests using the "stretched preflight slit function option" for the NO_2 fit. As can be seen in Sun et al. 2017 (Fig.3), the impact in the VIS is small (405-465 nm), and the row dependence is very weak. The impact on the NO_2 slant columns is almost zero.

8. P16, Figure 2, *what causes the relatively large difference between statistical and DOAS uncertainty in Northern high altitude in OMI data and in Southern high data in GOME-2 data?*

Figure 2 on Page 17 represents the differential HCHO slant columns themselves, not their respective statistical and DOAS uncertainties.

9. P17, L19, *does A only include absorption cross sections? How about the Jacobian for other parameters like wavelength shift?*

Matrix A is formed by the cross-sections and the measurements errors (which are largely random (noise)). Equation (4) does not take into account systematic errors, which are mainly dominated by slit function and wavelength calibration uncertainties, absorption cross-section uncertainties, by interferences with other species, or by uncorrected stray light effects (e.g. De Smedt et al., 2018). Uncertainties on estimated values of the nonlinear parameters (shift, stretch, intensity offset parameters) are not taken into account in the reported errors on the slant columns (Danckaert et al., 2017).

10. P17, L25, *you may add examples of non-linear parameters in the parenthesis.*

The shift, squeeze and intensity offset parameters are now added in the text as non-linear parameters (P18 L14)

11. P19, L8, *has V3.1 been released?*

Not yet. NASA has advised users to not use the v3.0 SCD uncertainties.

12. P20, Figure 3d, *why DOAS uncertainty for NASA algorithm does not change much with latitude? Have some of systematic uncertainties been removed in the fitting (e.g., destriping, common residuals) so that DOAS uncertainties are even smaller for 40S-40N?*

NASA DOAS uncertainties have indeed been post-processed, accounting for systematic effects. NASA removes common residuals from the OMI reflectances during the SCD retrieval. Moreover, such residuals are treated as solar zenith angle (thus latitude) dependent. This tends to dampen the latitudinal dependence of NASA DOAS uncertainties. In the NASA approach the error estimates are based on the statistics (chi-square estimates around the optimal SCD solution) primarily driven by the 'quality' of the OMI reflectances. Such quality depends on the effectiveness of instrument noise suppression via the removal of the common wavelength-, latitude- and FOV- dependent residuals.

13. P25, L19, *you may mention "cloud radiance fraction" typically larger than "cloud fraction" so that clear-sky values are still slightly larger than all-sky values.*

Thank you for your suggestion. The sentence: "Cloud radiance fraction values are typically larger than cloud fraction values therefore SCD uncertainties for clear-sky conditions are still slightly larger than the all-sky ones." is now added (P25 L23)

14. P29, L6-11, *it is interesting to note from Figure 8b that DOAS SCD uncertainties seem to be smaller for those extreme off-nadir pixels in OMINO2-QA4ECV product. Is this due to increasing viewing zenith angle that increases reflectance as a result of multiple scattering?*

The OMI rows excluded from our analysis are 22-53 (0-based). Therefore, relative to the "gap" on the maps, the row right before the gap starts (left side of the gap) is row 21 which is close to the absolute nadir viewing angle and this row appears the bluest (low uncertainty), whereas the row right after the gap ends (right side of the gap) is row 54 which is extreme off-nadir pixels and appears greenish (i.e. higher uncertainty).

15. P32, L13-15, *this sentence is not clear, suggest rephrasing it. For example, it is not clear whether using annual mean increases or decreases the strips by saying "it manifests"*

Good point. We now clarify that the presence of stripes is what manifests when we use annual mean solar irradiance spectra as reference (P32 L13).

16. P39, L33-34, *suggest rephrasing this sentence there is not cause-effect relationship between increasing SCD uncertainties and stability of stratospheric and tropospheric retrievals.*

We understand 'stability' here as defined by GCOS: stability is a requirement on the extent to which the uncertainty of a measurement remains constant over a long period. So if the SCD uncertainties increase over time, this affects the stability of the retrievals.

Technical comments

1. P6, L11, *change "absorption signature" to "absorption signatures"*
Done (P5 L15 and P7 L12)

2. P7, L3, *add "in" before "September"*
Done (P7 L8)

3. P11, L16, *change the second "stretch" to "squeeze"*
Done (P11 L25)

4. P14, L12, *change "prior" to "prior to"*
Done (P14 L12)

5. P19, L2, *change "extend" to "extent"*
Done (P19 L20)

6. P39, L27, *add "those" before "over bright scenes"*
Done (P40 L5)

Response to Anonymous Referee #3

We thank Anonymous Referee #3 for the evaluation and recommendations, which helped to improve the manuscript. In the following, a point-by-point reply is given, with the Referee comments in italic. Page and line numbers in the replies refer to the marked-up version of the manuscript.

Major: P7 L15: *Early in the manuscript, please consider discussing how the results presented for GOME-2A do or do not apply to GOME-2B, in general terms.*

We understand the point. But although there are some similarities between GOME-2A and GOME-2B, we find it difficult to extrapolate our findings to GOME-2B. We did not investigate spectral fits from GOME-2B, since it was not addressed in the QA4ECV-project. We therefore prefer to not speculate how our results may or may not apply to GOME-2B.

P13 L5: *What does this paper find regarding systematic variation of SCD with fit window size? Are there systematic differences between retrievals that use larger and smaller fit windows?*

We did not address this issue here, but we cite van Geffen et al. [2015] who showed that systematic differences may be of the order of 0.5×10^{15} molec. cm^{-2}, so that the reader can anticipate that differences in the fitting windows between GONO2A-BIRA (425-450 nm) and GONO2A-QA4ECV (405-465 nm) will contribute to the SCD differences shown in Figure 1 (right panel) (P16).
For more information on different fitting approaches, we refer to QA4ECV Deliverable 4.2 (www.qa4ecv.eu) [Müller et al., 2016] and Boersma et al., 2018 (in preparation).

P21 L2: *(Figure 4) This figure, and others like it in the manuscript, can be better represented in table format or text. As an example, the caption contains all of the pertinent information and the figure does not provide additional insight. In fact, I would think that table 4 also reflects the same information, but the 1-sigma uncertainty estimates are reported as different in table 4 and the caption of figure 4.*

We think that the Gaussian shape of the distribution shown in Figure 4 (P21) does provide the insight that the deviations around the mean SCD value are normally distributed, and most likely originate from measurement noise in level-1 data. This is an important argument in trusting the statistical approach to provide an independent value of the SCD uncertainty. If for instance there would be strong geophysical variability or systematic errors in the SCD values, we would not see a smooth Gaussian curve but a skewed distribution.

The values in Table 4 (P22) are the same (rounded) with those in Figure 4, which shows the same 1-sigma uncertainties under all-sky conditions, but for comparison, also those under mostly clear sky conditions.

P22 L17: *Is there a "partial cloud" impact on noise? I.e., is there more noise at some intermediate crf value? – After reading the paper in completion, I find that this discussion* *and results section is repeated in more detail later in the paper. E.g., you answer my above question in later section.*

We have no indications that noise would be higher for some intermediate cloud radiance fraction. In general, the impact of photon shot noise decreases with increasing cloud radiance fraction.

P24 L8-16: *Again, as with the above comment, results presented later in the manuscript provide a means to address what you have described here: you can compare OMI and GOME-2 uncertainty estimates in 2007 before GOME-2 degradation has accumulated. Please comment and consider arranging the text to combine the analysis (e.g., Figures 11-12, year = 2007).*

Thank you for this suggestion. We have added the sentence: "This is indeed the case for the early years of the instruments' mission; for 2007 the GOME-2A NO_2 SCD statistical uncertainty ($\approx 0.45\times10^{15}$ molec. cm^{-2}; Figure 11(left)) is lower than for OMI ($\approx 0.66\times10^{15}$ molec. cm^{-2}; Figure 9(c))." (P24 L15)

P33 L21: *Please report the HCHO behavior more precisely. This information would be useful to evaluate the discussion in p24 L8-16. See also Figure 12, Panels 1,3, year = 2007 (before degradation of GOME-2A)*

We added the sentence "The reduction of the uncertainty increase rate is even stronger for clear-sky scenes. GOME-2A HCHO SCD uncertainties show similar behavior; before the throughput test the uncertainty increases at a pace of 12-17%/yr (20%/yr reported for the UV) while after the test the increase rate is 1-4%/yr (3%/yr reported for the UV). " (P33 L21)

Figure 12 Panels 1-3: *Please comment briefly on why the OMI-BIRA has more uncertainty and GOME-BIRA has les uncertainty than its QA4ECV counterpart*

For QA4ECV OMI HCHO, the use of the larger fitting window, allowed for better determination of the least-squares problem, decreased the uncertainty in the slant columns. As explained in the text, we were expecting a similar effect for GOME-2, but the need to compensate for polarization effects in the large fitting window is found to offset the benefit of using a larger fitting interval.

P36 L15-L20: (a repeat of top-level concern) *This paragraph is one of the more important in the manuscript. It should be moved to its on section or combined with 4.3.4 "Implication for stability of long-term tropospheric measurements" and include more discussion. In particular, I am interested in the potential interferences of large scale geophysical variations such as stratospheric O3 or BrO variations on reported HCHO trends, which may depend on decadal and multi-decadal climate variability, and would not be well represented in the 2deg x 2deg empirical uncertainty estimates.*

We agree that the specificity of the GOME-2 retrieval algorithm should be described in the corresponding section. The in P14 (L16-24; pre-revision manuscript) is now updated with the inclusion of polarizations response cross-sections (eta and zeta) in the fit (P15 L3-17).

Concerning the impact of spectral interferences due to ozone and BrO absorption features (e.g. González et al., 2015)(which are largest under high latitude and low sun conditions), these are largely mitigated by the background correction scheme. Due to the nature of this correction, only non-zonal variations in ozone or BrO could lead to a substantial effect on the corrected HCHO columns. So only geographically localized trends in ozone or BrO that would also be coincident with HCHO emission regions could potentially affect the trends in corrected HCHO values, which is rather unlikely. So we believe that such effects, if any, cannot lead to substantial biases in HCHO trend analyses. Note also that trend studies are generally performed using monthly or even yearly averages so that the impact of random uncertainties (which increase with time in the case of GOME-2 due to throughput loss) become small, and in practice almost negligible in the uncertainty budget.
This being said, it is certainly correct that HCHO trend detection is generally more challenging with the GOME-2 instrument because of its stronger instrumental degradation (which notably affect random uncertainty but may also manifest itself in systematic effects possibly not perfectly mitigated by the background correction). In comparison OMI is better suited for trend studies owing to its exceptional radiometric stability.

A summary of this text is now included in the manuscript (P35 L5; P37 L6, 9)

P38 L20-22: *This proposed test would seem to fit well in this paper.*

Thank you for the suggestion. We investigated the time series of monthly means of tropospheric NO_2 columns from OMI and GOME-2A over the Pacific ocean (180°-220°E, 0°-10°N). We found that for both instruments the tropospheric columns appear stable in time with no significant trend (text added in Line 33 Page 38; figure added in Supplement (i.e. Figure S6)).

Minor P4 L29: *Is OMI a push-broom instrument? I thought it was a 2-D CCD.*

OMI observes solar backscatter radiation in a push-broom mode with a telescope that feeds two (one for the UV, one for the VIS) imaging spectrometers. Each spectrometer employs a 2D (spatial and spectral information obtained simultaneously) CCD detector (e.g. Levelt et al., 2018).

P5 L26: *Does the row-position of stripe maxima vary over time? If so, with what time constant? Each orbit? Each day?*

The stripe-correction for each row does not change from orbit to orbit, nor from day to day. Even after several days (e.g. a month) the pattern and the values of the stripe correction will be by and large the same, see Boersma et al. [2011]. Large time scales are required for the stripe correction to change significantly (e.g. Figure 10(left); P32).

P6 L15: *AMF = 4 is very large for HCHO and tropospheric NO_2. I suggest use of a smaller value.*

A value of 4 for the AMF is indeed not a typical value for a polluted scene, but here we are concerned with typical background scenarios. Even if we choose a smaller value for the AMF, the optical thickness of HCHO is 10× smaller than the one of NO_2 rendering HCHO detection more difficult.

P6 L28: *Is there a reference literature on the GOME instrument to include here?*

A reference in literature for GOME-2A (i.e. Callies et al., 2000) is mentioned in Line 29 (Page 6).

P8 L21: *"sensitivity to the absorber of interest" Add reference that does a good fit window optimization.*

We added the following references: González et al., 2015; QA4ECV Deliverable 4.2 [Müller et al., 2016]; Liu et al., 2016 (P8 L26)

P12 L24: *"better represent the across-track average" Does the updates algorithm use a unique slit function for each cross-track position? It seems like this sentence is saying that one slit function is used for all cross-track positions.*

In OMNO2A v1, a fixed slit function for all rows was used. In OMNO2A v2, the wavelength and viewing angle dependency of the slit function are taken into account in the form of a row-average slit function. See van Geffen et al. [2015].

P12 L32: *"but is largely identical to the approach taken" Please clarify. Also, please either remind reader why different parts of data record are processed with different algorithms (NLIN and QDOAS), or if it is not important, omit.*

"But" is now changed to "and" to avoid contrast and confusion (P13 L10). Any differences between the approaches are described in Table 2 (P9).

NLIN and QDOAS have been tested on the same data and have delivered very consistent results (QA4ECV Deliverable 4.2 [Müller et al., 2016]). In view of this excellent agreement and the need to share the burden of processing tasks, 2007-2011 was processed with NLIN and 2008-2016 was processed with QDOAS (reasoning added in Line 16- P10). We prefer to keep this detail as a footnote in Table 2 for transparency.

P14 L12: *Why are cross-sections dynamically convoluted with slit function for HCHO fit but not for NO_2?*

This is due to the fact that, as discussed in Sun et al 2017, the "preflight slit function" differs more from the "stretched preflight slit function" in the UV than in the VIS. The same holds for the GOME-2 slit function, that also changed significantly over time in the UV and much less in the VIS.

P14 L22: *Please briefly expand on "E/W bias in the extended fitting interval." I do not understand as written.*

In the large fitting window, a scan angle dependent spectral signature from a polarization sensitivity of the GOME-2 instrument which is not fully removed by the calibration of the level-1 data results in a scan angle dependency of the retrieved HCHO slant columns. The spectral structure can be extracted by comparing the residuals of fits from different viewing directions over regions with known and homogeneous HCHO columns as shown for OClO in (Richter et al., EGU General Assembly, 2016). When adding the extracted spectral signature as additional cross-section in the retrieval, most of the scan angle dependent bias is removed.

P17 L2: *Please remind the reader more precisely what is meant by "background correction." Is this the correction for using a radiance reference spectrum?*

This concerns the global HCHO background correction as described in Eq. (1) in De Smedt et al. [2018]: subtraction of the mean HCHO per row (across-track correction) and by 5° latitudinal bins (along-track correction). This correction ensures that the HCHO differential SCDs over the Pacific Ocean reference sector are approximately zero. They are subsequently corrected by adding a background vertical column from the TM5-MP Model.

The background correction is described in detail in De Smedt et al. [2018].

P18 L18: *How are clouds treated in this analysis? Are all data included? You describe in more detail later, but a brief comment here would be useful.*

Thank you. We now explicitly say that we investigate all-sky and clear-sky (cloud radiance fraction < 0.5) conditions (P19 L6).

P19 L7-10: *Why does this discussion begin with NASA NO_2 product? It's the fourth panel of the relevant figure and is the last item for discussion at other points in the paper. It makes for a rough transition. Please better reference Figure 3 panels in the text to help the reader. Also, please comment briefly on the suspected cause of the 0.5 x 10ˆ15 systematic difference between v3.0 and v3.1 as this is a large value relative to the errors discussed in this paper.*

Thank you for pointing this out. Lines 7-10 in P19 (pre-revision manuscript) have now been moved to P15 L28. We now also provide an explanation of the differences between the two NASA versions. The OMNO2-NASA SCDs (and their uncertainties) used in this analysis correspond to v3.1 of the new Standard Product (SP) (Krotkov et al. [2017]). Over the chosen clean-sector area the v3.1 SCDs are on average higher by ~0.5×10^{15} molec. cm^{-2} than v3.0. Differences between v3.1 and v3.0 SCD values are related to the changed approach to flagging of the presumably noisy wavelength bins in the OMI radiances, as well as improved solar reference spectra.

Then we moved lines 10-11 in P19 (pre-revision manuscript) to P21 L5, and added an explanation of the differences between versions. The OMNO2-NASA v3.1 DOAS SCD uncertainties are on average 40% lower than v3.0. This reduction of the DOAS SCD uncertainties stems from correction of an error in the v3.0 algorithm. The statistical SCD uncertainties are similar between v3.1 and v3.0 (agreement within 0.02×10^{15} molec. cm^{-2}).

<u>P21 L17-21:</u> *This sentence should be moved to section 4.2. Alluding to results discussed later in the paper distracts from the narrative. I also was unclear what was meant by "on a global scale"*

This is a fair point. We have removed the sentence.

The "on a global scale" phrase is now added in Line 8 (P29). The uncertainty analysis in this manuscript is based on the Pacific region, where we see the improvement of the DOAS SCD uncertainties from QA4ECV relative to OMNO2A. We see such improvement also on a global scale, and not only over the Pacific.

<u>P33 L13:</u> *How is ISRF different from slit function? Unless this difference is important to outcomes of this paper, please avoid introducing extraneous jargon and acronyms.*

Thank you. We now replaced "ISRF" with "slit function" (P33 L13).

<u>P37 L10-19</u>: *The GCOS discussion of error and uncertainty estimates may be more useful to the reader if moved earlier in the manuscript.*

We have considered this suggestion. If we place the GCOS discussion earlier in the text, we run the risk of leading the reader away from the uncertainty analysis. We believe we should discuss GCOS requirements after all results are presented and the analysis is complete.

<u>P37 L24:</u> *"If we consider the SCD uncertainties to be completely systematic in nature" Please clarify this discussion. Based on the empirical analyses, we know that there is some large fraction of the uncertainty that is randomly distributed. I would prefer if the authors referred to "SCD uncertainties" that are "systematic in nature" to be "systematic errors."*

Thank you, we realize that "in nature" may cause confusion. It is now removed (P38 L11).

<u>P38 L28:</u> *"structural uncertainties may increase up to 30-40%" as evaluated over what time period?*

The percentages 30% and 40% correspond to OMI orbits on 16 August 2005 and 2 February 2005, respectively (Lorente et al., 2017).

<u>Suggested edits for word choice, word order and grammar (non-exhaustive list)</u>

<u>P2 L21:</u> *"reliable and traceable information on data quality"*

Done (P2 L22)

<u>P3 L3:</u> *"Here, we quantify : : :"*

Done (P3 L4)

P5 L14: *Replace “jumps” with “non-physical variation”, “variation” or “cross-track variation”*

Done (P5 L18)

P5 L33: *“We exclude the affected rows : : : from our analysis”*

Done (P6 L4)

P6 L8: *Delete “Together with : : : performance, its”. Add “OMI”*

Done (P6 L13)

P6 L24: *“node” – “orbit”*

Done (P7 L1)

P8 L15: *Here and through the manuscript, I do not understand the parantheses around certain adjectives. “Signal” or “observed signal” are better than “(observed) signal”*

The parenthesis is now removed (P8 L20)

P11 L16: *repeated use of “stretch”*

We now use “squeeze” instead of stretch (when $\omega_q < 0$) (P11 L25)

P16 L9: *Here and throughout, I recommend using consistent nomenclature in both equations and text, replacing all instances of SCD in the text with N_s and vertical column with N_v.*

SCD and VCD are generally common abbreviations in the DOAS community, so we like to stick to them. Since SCD or VCD are not mathematical symbols, we do not use them in any of the equations, and use N_s and N_v to describe these terms.

P17 L11-14: *Please clarify this sentence. What is “this routine”? and what is a “mostly linear fit”?*

In Lines 23-24 (P17), we refer to the M-L procedure as “the routine”.

The QDOAS fit contains also non-linear parameters (shift, stretch, offset parameters) therefore its linearity is broken down.

P24 L19: *“pronounced absorption signatures” + “large abundance in the atmosphere” and “relatively small differential optical depth” contradict one another. The latter is the important point to communicate.*

We realize the confusion. The phrases “pronounced absorption signatures” and “relatively large abundance” are now removed (P24 L26).

<u>P33 L14</u>: *"ISRF changes are strongly weakened" - evaluate word choice*

"Strongly" is now replaced by "considerably" (P33 L15)

<u>P37 L21</u>: *"(e.g., the systematic reductions in SCDs by +/- 1.2x10ˆ15)" Is the plus minus sign incorrect or is the sentence intended to say SCD uncertainties?*

It is not replaced with a different sign to avoid confusion (P38 L8)

<u>Last remarks (1/2):</u> *I do not necessarily see the value of including footnotes. In most cases in this manuscript the footnotes do not add value (footnote 1, 2,) or could be better addressed in line with the text (footnote 3)*

In literature one can find different definitions of a measurement uncertainty. Since this manuscript is devoted to uncertainties, we feel obliged to provide an accurate definition (as does footnote 1; P3) according to the GUM (Guide to the Expression of Uncertainty in Measurement) and the VIM (International Vocabulary of Basic and General Terms in Metrology).

We agree that Footnote 2 (P4) that briefly describes the "SAOZ" instrument should be removed.

We feel that if we move footnote 3 (P8) we will disrupt the flow of the text that describes the concept of the DOAS technique.

<u>Last remarks (2/2):</u> *Regarding readability, I would find ways to condense what has been written by decreasing repetition.*

Figures 5(a) and (b) (P23; pre-revision manuscript) are now removed. The message they convey is inline. Figure 5(c) is now the new Figure 5 (P23).

Improved slant column density retrieval of nitrogen dioxide and formaldehyde for OMI and GOME-2A from QA4ECV: intercomparison, uncertainty characterization, and trends

Marina Zara[1], K. Folkert Boersma[1,2], Isabelle De Smedt[3], Andreas Richter[4], Enno Peters[4], Jos H. G. M. van Geffen[1], Steffen Beirle[5], Thomas Wagner[5], Michel Van Roozendael[3], Sergey Marchenko[6], Lok N. Lamsal[6], and Henk J. Eskes[1]

[1] Royal Netherlands Meteorological Institute (KNMI), De Bilt, the Netherlands
[2] Wageningen University~~ & Research (~~,WUR~~)~~, Meteorology and Air Quality Group, Wageningen, the Netherlands
[3] Institut royal d'Aéronomie Spatiale de Belgique, BIRA-IASB, Belgium
[4] Institut für Umweltphysik, IUP, Bremen, Germany
[5] Max-Planck-Institut für Chemie, MPI, Mainz, Germany
[6] Goddard Space Flight Center, NASA, Greenbelt, United States

Correspondence to: Marina Zara (marina.zara@knmi.nl)

Abstract.

Nitrogen dioxide (NO_2) and formaldehyde (HCHO) column data from satellite instruments are used for air quality and climate studies. Both NO_2 and HCHO have been identified as precursors to the ozone (O_3) and aerosol Essential Climate Variables, and it is essential to quantify and characterize their uncertainties. Here we present an intercomparison of NO_2 and HCHO slant column density (SCD) retrievals from 4 different research groups (BIRA-IASB, IUP, and KNMI as part of the Quality Assurance for Essential Climate Variables (QA4ECV) project consortium, and NASA) and from the OMI and GOME-2A instruments. Our evaluation is motivated by recent improvements in Differential Optical Absorption Spectroscopy (DOAS) fitting techniques, and by the desire to provide a fully traceable uncertainty budget for climate data record generated within QA4ECV. The improved NO_2 and HCHO SCD values are in close agreement, but with substantial differences in the reported uncertainties between groups and instruments. As a check of the DOAS uncertainties, we use an independent estimate based on the spatial variability of the SCDs within a remote region. For NO_2, we find the smallest uncertainties from the new QA4ECV retrieval (0.8×10^{15} molec. cm^{-2} for both instruments over their mission lifetimes). Relative to earlier approaches, the QA4ECV NO_2 retrieval shows better agreement between DOAS and statistical uncertainty estimates, suggesting that the improved QA4ECV NO_2 retrieval has reduced but not altogether eliminated systematic errors in the fitting approach. For HCHO, we reach similar conclusions (QA4ECV uncertainties of 8-12$\times10^{15}$ molec. cm^{-2}), but the closure between the DOAS and statistical uncertainty estimates suggests that HCHO uncertainties are indeed dominated by random noise from the satellite's level-1 data. We find that SCD uncertainties are smallest for high top-of-atmosphere reflectance levels with high measurement signal to noise ratios. From 2005 to 2015, OMI NO_2 SCD uncertainties increase by

1-2%/yr related to detector degradation and stripes, but OMI HCHO SCD uncertainties are remarkably stable (increase <1%/yr), related to the use of Earth radiance reference spectra which reduces stripes. For GOME-2A, NO_2 and HCHO SCD uncertainties increased by 7-9%/yr and 11-15%/yr, respectively, up until September 2009, when heating of the instrument markedly reduced further throughput loss, stabilizing the degradation of SCD uncertainty to <3%/yr for 2009-2015. Our work suggests that the NO_2 SCD uncertainty largely consists of a random component (~65% of the total uncertainty) ~~(~~as a result of the propagation of measurement noise~~)~~, but also of a substantial systematic component (~3~~0~~5% of the total uncertainty) mainly from “stripe effects”. Averaging over multiple pixels in space and/or time can significantly reduce the SCD uncertainties. This suggests that trend detection in OMI and GOME-2 NO_2 and HCHO time series is not limited by the spectral fitting, but rather by the adequacy of assumptions on the atmospheric state in the later air mass factor calculation step.

1 Introduction

Nitrogen oxides (NO_x = NO + NO_2) and formaldehyde (HCHO) play important roles in atmospheric chemistry by driving the formation of ~~ozone~~O_3 (e.g. Sillman et al., 1990) and aerosols (e.g. Bauer et al., 2007), and influencing hydroxyl (OH) concentrations in the global troposphere (e.g. Miyazaki et al., 2017). Surface atmospheric concentrations of NO_2 may reach levels that are directly harmful to health (e.g. Fischer et al., 2015) and lead to detrimental environmental impacts through acid rain. Formaldehyde is a known carcinogen (e.g. Zhu et al., 2017). Observations of NO_2 and HCHO are thus important for air-quality monitoring and forecasting as well as climate (IPCC, 2013). Recently, the Global Climate Observation System (GCOS) has identified NO_2 and HCHO as precursors to Essential Climate Variables (ECVs) because of their value in detecting and attributing changes in ~~ozone~~O_3 (e.g. Verstraeten et al., 2015) and aerosol distributions (GCOS-138, 2010).

Satellite instruments are providing long-term global records of tropospheric NO_2 and HCHO column densities, as well as stratospheric NO_2, but there is a need still for reliable and traceable ~~quality~~ information on data quality. The EU FP7-project Quality Assurance for Essential Climate Variables (QA4ECV) (http://www.qa4ecv.eu/) is addressing this need by providing a fully traceable quality assurance effort on all aspects of the NO_2 and HCHO (and carbon monoxide) retrieval algorithms. Spectral fitting is the first step in the algorithms used for the retrieval of NO_2 and HCHO columns (e.g. Leue et al., 2001; Richter et al., 2011; De Smedt et al., 2012). Using the Differential Optical Absorption Spectroscopy (DOAS) method, a modelled reflectance spectrum is matched to a satellite-measured reflectance spectrum to determine the abundance of NO_2 and HCHO along the average photon path between the Sun and the satellite, the so-called slant column density (SCD) of the trace gas. The total SCD may consist of a tropospheric and a stratospheric part. In the second step of the retrieval, a separation of the two parts occurs. One procedure to do so is via data assimilation in a Chemistry Transport Model (CTM), which estimates the stratospheric NO_2 vertical column density (VCD). Other alternative approaches estimate the stratospheric column directly from the satellite total column measurements over remote regions and above mid-altitude clouds, without input from CTMs (Bucsela et al., 2013; Beirle et al., 2016). The stratospheric NO_2 SCD is then subtracted from the total SCD yielding the tropospheric NO_2 SCD. In the final step the SCDs are converted to VCDs by dividing by the air mass factors (AMFs). An earlier study within the QA4ECV project focused on characterizing and quantifying the uncertainties associated with the NO_2 and HCHO AMF calculation (Lorente et al., 2017). Here, ~~our topic is the quantification of~~ we quantify the uncertainties of state-of-science spectral fitting algorithms for the NO_2 and HCHO SCDs from the Ozone Monitoring Instrument (OMI), aboard the EOS Aura satellite, and the Global Ozone Monitoring Experiment-2 (GOME-2) aboard the MetOp-A satellite.

Recently, spectral fitting procedures for NO_2 have been revised to accommodate improved information on absorption cross-sections, instrument calibration, and surface effects (Richter et al., 2011; Marchenko et al., 2015; Van Geffen et al., 2015; Anand et al., 2015; Krotkov et al., 2017). Based on extensive comparisons of spectral fitting approaches between BIRA-IASB, the University of Bremen (IUP), MPIC, and KNMI, the QA4ECV-consortium has developed improved spectral fitting algorithms for NO_2 and HCHO which have been tested and applied to spectra from OMI, GOME-2A, SCIAMACHY, and GOME (QA4ECV Deliverable 4.2~~, 2016~~ [Müller et al., 2016]; www.qa4ecv.eu). Here we will evaluate results from the new QA4ECV algorithm against existing SCD datasets, with special attention to characterizing the uncertainties in the datasets.

The issue of slant column uncertainty[1] remains relevant for NO_2 retrievals because it dominates the overall retrieval uncertainty over low and moderately polluted areas (Boersma et al., 2004). For HCHO, SCD uncertainties are substantial also over regions with enhanced concentrations, and averaging multiple observations in time or over a larger area is required in order to bring down the random fluctuations in the retrievals (e.g. Millet et al., 2008; Dufour et al., 2009) to a level that they can be used for applications such as trend analysis and emission estimates. Previous studies have quantified SCD uncertainties from GOME (Boersma et al., 2004), GOME-2 (Valks et al., 2011; De Smedt et al., 2012), and OMI (Boersma et al., 2007; Millet et al., 2008) for short periods of time, so it is unclear how the SCD uncertainties evolve over time, which is particularly relevant for instruments with substantial degradation in the quality of level-1 (ir)radiances such as GOME-2A (e.g. Dikty and Richter, 2011; Munro et al., 2016). Furthermore, the main drivers of the SCD uncertainties need to be identified to inform data users on where and when SCDs are most reliable, and to which extent averaging or filtering is required to bring down retrieval noise to render the data useful for applications.

Our study on the quality assurance of NO_2 and HCHO SCDs therefore has three coherent goals:

[1] Uncertainty is defined as a non-negative parameter that characterizes the dispersion of values attributed to a measured quantity (e.g.~~i.e~~. SCD). There is also uncertainty associated with the method of measurement, as there can be other methods (i.e. different spectral fitting algorithms), that would give systematically different results of apparently equal validity. This definition follows the guidelines of the Guide to the Expression of Uncertainty in Measurement (GUM; https://www.bipm.org/utils/common/documents/jcgm/JCGM_100_2008_E.pdf) and the International Vocabulary of Basic and General Terms in Metrology (VIM; https://www.bipm.org/utils/common/documents/jcgm/JCGM_200_2012.pdf).

1. Evaluate NO_2 and HCHO retrievals (from BIRA-IASB, IUP, KNMI, NASA, QA4ECV) by quantifying and characterizing the DOAS-derived SCDs and their uncertainties,
2. investigate the dependencies of the DOAS-derived SCD uncertainties,
3. analyse how SCD uncertainties develop over time, and how instrument degradation affects the stability of long-term climate data records.

The DOAS technique provides SCDs along with an uncertainty estimate for each spectral fit. The SCD uncertainties computed by DOAS are challenging to validate because direct independent reference measurements (of SCDs) are lacking. In principle, ground-based DOAS or SAOZ~~[2]~~ (Pommereau and Goutail, 1988) measurements can be used for validation, but they first require separate AMF conversions, corrections for mismatches in time, and careful consideration of differences in vertical and spatial representativeness of the satellite and ground-based measurements. In this paper, we therefore use an independent *a posteriori* method to establish the absolute level of the uncertainty in the NO_2 and HCHO SCDs that can be attributed to instrument noise in the level 1 data from OMI and GOME-2. This technique, first used by Wenig et al. [2001] and later by Boersma et al. [2007], translates the spatial variability in the slant columns over confined pristine areas with known limited geophysical variability (Pacific Ocean) into an uncertainty estimate for the slant columns itself. We concentrate on quality assurance of the most recent OMI and GOME-2 NO_2 SCD data sets from QA4ECV (QA4ECV Deliverable 4.2~~, 2016~~ [Müller et al., 2016]), KNMI (Van Geffen et al., 2015), and NASA (Marchenko et al., 2015), and on OMI and GOME-2A HCHO from QA4ECV (Deliverable 4.2~~, 2016~~ [Müller et al., 2016]) and BIRA-IASB (De Smedt et al., 2012; De Smedt et al., 2015).

Section 2 introduces the OMI and GOME-2A instruments, and discusses known issues with the quality of the level-1 data in the UV/VIS windows affecting the SCD uncertainties. Section 3 presents the currently operational spectral fitting algorithms for NO_2 and HCHO retrievals, and the main differences between the fitting approaches from different groups. Section 4 presents the intercomparison of the absolute SCDs retrieved from all fitting algorithms. We describe our method for an independent *a posteriori* SCD uncertainty estimation, followed by the evaluation of the DOAS SCD uncertainty with the statistical method. This section also investigates dependencies of the SCDs on potential drivers such as the SCD itself, AMFs, cloud fractions or top-of-atmosphere reflectances. Additionally, a trend analysis of the SCD uncertainty derived from the DOAS and the statistical technique over the 2005-2015 period is presented. We also discuss whether NO_2 and HCHO retrievals from OMI and GOME-2 can meet the GCOS requirements (http://www.wmo.int/pages/prog/gcos/) for satellite-based data products for climate, such as spatiotemporal resolution and instrumental stability. Finally, Section 5 summarizes our findings and discusses directions for future research.

~~[2] The SAOZ (Système d'Analyse par Observation Zénithale) spectrometer is a passive remote-sensing instrument that automatically measures ozone and NO_2 total VCDs up to the polar circle. The SAOZ observes the zenith sky with a field of view of around 30°, measuring light scattered downwards from a range of altitudes.~~

2 Quality of Level 1 data for UV/VIS sensors

2.1 Ozone Monitoring Instrument

The Dutch-Finnish Ozone Monitoring Instrument (Levelt et al, 2006b) is a push-broom nadir-viewing near-UV/Visible spectrometer aboard NASA's EOS Aura spacecraft launched in July 2004. In an ascending sun-synchronous polar orbit, crossing the equator at 13:40 hrs local time, OMI provides measurements of various trace gases, NO_2 and HCHO among them, along with ancillary information on UV-B surface flux, cloud and aerosol parameters. The instrument is equipped with two two-dimensional Charge Coupled Device (CCD) detectors (Dobber et al., 2006) for simultaneous spatial and spectral registration; CCD1 covers spectral channels UV1 (264-311 nm) and UV2 (307-383 nm) and CCD2 covers the VIS-channel (349-504 nm). It is in the latter channel that the spectral features of NO_2 are most prominent, while the UV2-channel is used for retrieving HCHO SCDs. With a spectral resolution (full width at half maximum) between 0.42 nm and 0.63 nm and a spatial resolution of 13×24 km^2 at nadir, OMI simultaneously measures the solar backscattered irradiance in a swath of 2600 km at every given orbital exposure, so that 60 pixels are simultaneously registered across track. OMI is equipped with a scrambler that depolarizes the light entering the spectrometers. The instrument signal-to-noise ratio in the OMI VIS and UV2 channels for clear-sky, dark scenes is such that the spectral fitting of typical differential absorption signatures is possible for NO_2 (absorption signatures comparable to noise in the reflectances), and challenging for HCHO (absorption signatures weaker by one order of magnitude than noise), see Table 1.

Since the beginning of the OMI mission, ~~jumps~~ non-physical variation in SCD values from one viewing angle (i.e. at a given cross-track position, or OMI 'row' hereafter) relative to another have been observed in both the NO_2 and HCHO data. These small, discrete jumps result in "stripes" along the orbit. The origin of the stripes is not well known, but it is probably related to small differences in wavelength calibration for each of the 60 viewing angles, and to noise and instrument-related artefacts (e.g. the relatively low-amplitude spectral features introduced by the solar diffuser) in the solar irradiance spectrum used in the computation of the reflectance (Boersma et al., 2011; Veihelmann and Kleipool, 2006; N. Rozemeijer, priv. comm., 2017). Stripes appear as a systematic effect along the orbit, and it is possible to correct for them following an a posteriori "de-striping" procedure that is based on the premise that geophysical variation in NO_2 or HCHO in the across-track direction (East-to-West) is smooth rather than stripe-like (Boersma et al., 2007). The NO_2 de-striping corrections (for the OMNO2A retrievals in the DOMINO v2 processing system) are generally of the order of 0.3-0.5×10^{15} molec. cm^{-2}, which is within 10% of typical SCD values, but have grown in time (Boersma et al., 2011). Weaker absorbers like HCHO are affected more by this instrumental artefact (up to 50×10^{15} molec. cm^{-2}), but the use of daily radiance spectra as reference (instead of solar irradiance spectra) reduces the stripes in the OMI HCHO SCDs (down to 2×10^{15} molec. cm^{-2}) (e.g. De Smedt et al., 2015).

Apart from the stripes, OMI measurements contend with the "row anomaly" (RA), a dynamic effect first noticed in June 2007 when several cross-track FOVs (rows) began to experience partial blockage of incoming Earth radiance. Since then, the

RA extended to other rows (https://disc.sci.gsfc.nasa.gov/Aura/data-holdings/OMI; see more discussion in Schenkeveld et al., 2017). This RA mostly appears as a signal suppression in the level 1B radiance data at all wavelengths, leading to cloud retrievals of poor quality, even though successful spectral fits for NO_2 and HCHO can still be achieved (QA4ECV Deliverable 4.2~~, 2016~~ [Müller et al., 2016]). We exclude ~~here from our analysis~~ the affected rows 22-53 (0-based) from the entire orbit throughout the 2005-2015 period from our analysis.

In spite of the above issues, OMI's radiometric stability is very good for a UV-Vis spectrometer. It is monitored by routine measurements of solar flux, and by tracking on-board parameters (Dobber et al., 2008) and geophysical parameters (e.g. average reflectivity in Antarctica and Greenland) (McPeters et al., 2015). Over the period 2004-2010 the optical degradation in the visible channel was less than 2% (Boersma et al., 2011), and remains below 2% up to this day (see Sect. 4.3.1). Schenkeveld et al. [2017] report 1-2% radiance (practically ~~achromatic~~wavelength independent) and 3-8% irradiance (slightly wavelength-dependent) degradation over the mission, and the wavelength calibration of the instrument remaining stable to 0.005–0.020 nm. ~~Together with OMI's good performance, its~~ OMI data are considered to be reliable and of good quality for the full mission thus far.

Table 1. Estimated signal-to-noise ratio (SNR) for OMI and GOME-2A in the UV and VIS channels for one pixel. The uncertainties in the logarithm of the reflectances are based on the SNR for the radiance and a relatively dark, clear-sky planetary scene with a TOA reflectance assumed to be 0.2 (or 0.8×10^{13} photons$\cdot$sr$^{-1}\cdot$s$^{-1}\cdot$nm$^{-1}\cdot$cm^{-2}) for the UV2-channel and 0.1 (1.3×10^{13} photons$\cdot$sr$^{-1}\cdot$s$^{-1}\cdot$nm$^{-1}\cdot$cm^{-2}) for the VIS-channel. The differential optical thickness was calculated for a scenario with 10×10^{15} molec. cm^{-2} HCHO and 10×10^{15} molec. cm^{-2} NO_2 and a total AMF of 4.

	SNR radiances 340-360 nm	noise on $\ln(I/I_0)$	Differential optical thickness HCHO	SNR radiances 400-470 nm	noise on $\ln(I/I_0)$	Differential optical thickness NO_2
OMI	400[a]	2.5×10^{-3}	3×10^{-4}	500[a]	2×10^{-3}	2×10^{-3}
GOME-2A	1000[b]	1×10^{-3}	3×10^{-4}	1000[b]	1×10^{-3}	2×10^{-3}

[a]Based on globally averaged OMI lv1 radiance SNR levels recorded for orbit 21078 (1 July 2008) (Q. Kleipool, priv. comm., 2017). The SNRs in the OMI irradiance (reference spectra used for retrievals (e.g. yearly averages in the OMNO2A v1, v2 approach)) are much higher, 2000 for UV2 and 4000 for VIS, that it is neglected in the calculation of the uncertainty of the logarithm of the reflectance.

[b]This estimate (for 2007) is based on the level-1 radiance levels mentioned in the Table caption and signal-to-noise vs. lv1 curves for GOME-2A Band 4 and Band 5 obtained from R. Lang (priv. comm., 2017).

2.2 Global Ozone Monitoring Experiment-2

The Global Ozone Monitoring Experiment-2 (Callies et al., 2000) onboard EUMETSAT's METOP-A satellite (GOME-2A) was launched in October 2006 into a Sun-synchronous orbit, crossing the equator at 09:30 hrs local time in the descending

~~node~~orbit. GOME-2A is a whisk-broom UV-Visible spectrometer measuring solar irradiance and Earth radiance in the nadir swath with ground pixels of 40 km along track and 80 km across track using a scanning mirror to measure 24 such scenes across the 1920 km wide swath, followed by 8 larger (240×40 km^2) back-scan pixels. Nearly global coverage is obtained daily with small gaps in the equatorial regions. GOME-2A records spectra in the range from 240 to 790 nm at a spectral resolution of 0.26-0.51 nm, allowing the retrieval of the same atmospheric components as OMI, as well as sun-induced fluorescence (e.g. Joiner et al., 2013; Sanders et al., 2016). Additionally, two polarization components are retrieved with polarization measurement devices (PMDs) at 30 broad-band channels covering the full spectral range. From 15 July 2013 onwards, GOME-2A operates in tandem with its accompanying sensor GOME-2B (launched in September 2012) with a reduced swath of 960 km and pixels of 40x40 km^2 (Munro et al., 2016), motivated by the desire to monitor global air quality on a daily basis with the two sensors. The GOME-2A signal-to-noise ratio in band 4 (UV) and band 5 (VIS) was (initially) better than for OMI, so that spectral fitting of typical differential absorption signatures is quite feasible for NO_2 (with a signature ~2× stronger than the noise in reflectances), and possible for HCHO (absorption signatures weaker than noise but of comparable magnitude still - see Table 1).

Since the GOME-2A launch, the quality of its level-1 data seriously degraded due to: (1) instability of the instrument slit function (e.g. Dikty and Richter, 2011; De Smedt et al., 2012), (2) potential degradation in the reflectance noise because of solar diffuser degradation, (3) the instrument throughput loss, and (4) polarization spectral structures in the UV channel. All these potentially influence the spectral fitting of HCHO and NO_2 in the GOME-2A measurements. We discuss these issues in more detail below, since they are important in understanding the uncertainties associated with the HCHO and NO_2 SCD retrievals from GOME-2A.

The GOME-2A slit function varies seasonally and fluctuations are larger in the UV than in the visible, with the width of the slit function narrowing over time (e.g. FWHM reductions of 8% at 359 nm and 6% at 429 nm between 2007-2015 (e.g. Lacan and Lang, 2011; Dikty and Richter, 2011, De Smedt et al., 2012; Munro et al., 2016)). These variations are mostly related to the thermal fluctuations of the GOME-2A optical bench associated with seasonal and long-term changes in the solar irradiance (Munro et al., 2016). Changes in the slit function shape due to inhomogeneous slit illumination are not considered to be an issue due to the averaging effect caused by across-track scanning (Munro et al., 2016). The calibration of the GOME-2A solar irradiance measurements is different from that of the radiances, because the irradiances are reflected by the solar diffuser before arriving at the scan mirror. This additional optical component (relative to the radiance light path) implies that any inadequacies in the characterization of the diffuser or changes during the mission lead to degradation of the reflectances. To avoid these issues, but also the degradation in radiances and in scan angle dependent calibration knowledge, radiance measurements over a reference location are used instead of irradiances for GOME-2A HCHO SCD retrievals (e.g. De Smedt et al., 2012).

The degradation of other optical components in the GOME-2A instrument resulted in a progressive wavelength-dependent loss of the instrument throughput. The throughput losses are more pronounced in the UV (around 20%/yr) than in the visible (10%/yr) (EUMETSAT: Investigation on GOME-2A Throughput Degradation, 2011). The main impact of the degradation on the DOAS retrievals is an increase of the noise due to throughput loss. EUMETSAT issued throughput tests in January and September 2009 in order to understand the mechanisms responsible for this degradation and define actions to control it. The second test caused an additional decrease in throughput of 25% in the UV and 10% in the visible relative to January 2007, but has also stabilized GOME-2A degradation, with a reported degradation rate of 3%/yr for the UV channel and 1%/yr for the visible after September 2009. Based on knowledge of the signal strength loss, we ~~may~~ expect the random uncertainties of the SCDs to increase with time throughout the mission, but especially before September 2009. We will discuss this aspect further in Section 4.3.

3 DOAS technique

All retrievals in this work use the DOAS technique (Platt, 2017), which is based on the Lambert-Beer law, describing the attenuation of light passing through a medium. It determines the trace gas concentrations integrated along the effective photon path in the atmosphere by identifying the relative depth of their characteristic absorption fingerprints. The technique discriminates the spectrally smooth component of radiation attenuation (e.g. from Rayleigh and Mie scattering, variable surface reflectance, spectrally changing instrument throughput) from the attenuation from molecular absorption, which has distinct spectral features. In DOAS, a high-pass filter (nominally a low order polynomial) of the spectra eliminates these broadband extinction processes. Also reference spectra to describe the effects of rotational Raman scattering (the so-called "Ring effect") are included. The ~~(~~observed~~)~~ signal that varies rapidly with wavelength is matched to a modelled spectrum based on reference spectra (i.e. lab-measured cross-section spectra) of the trace gases of interest. For this purpose, a model spectrum is constructed that approximates the observed reflectance spectrum ($R_{obs}(\lambda) = \frac{\pi I(\lambda)}{\mu_0 I_0(\lambda)}$ with $I(\lambda)$ the earth radiance spectrum, $I_0(\lambda)$ the reference spectrum, usually from the Sun, and μ_0 the cosine of the solar zenith angle[3]), or the natural logarithm of the observed reflectance spectrum, which is proportional to the optical depth ($\tau(\lambda) = \ln\left(\frac{I_0(\lambda)}{I(\lambda)}\right)$). The DOAS-technique then minimizes the differences between the modelled and the observed spectra within a pre-defined spectral or fitting window with optimal sensitivity to the absorber of interest (e.g. González et al., 2015; QA4ECV Deliverable 4.2 [Müller et al., 2016]; Liu et al., 2016). Those coefficients that minimize the differences between the model and the observations are retained as slant column densities for a given trace-gas species. Minimization of the differences between

[3]In OMNO2A and QA4ECV-QDOAS algorithms (see Section 3.1.1), the impact of the solar zenith angle at which the backscattered light is measured is taken into account in the viewing geometry (i.e. AMF) of the measurement and the polynomial in the fit (See Section 3.1.1). A successful fit can be achieved even when measurement occurs at 90° solar zenith angle (μ_0 = 0) by using $R_{obs}(\lambda) = \frac{I(\lambda)}{I_0(\lambda)}$ as observed spectra instead.

modelled and observed reflectances is usually called ‘intensity fit’, between modelled and observed optical depths an ‘optical depth fit’.

3.1 NO_2 slant column density retrievals

3.1.1 OMI NO_2 spectral fitting and SCDs

Table 2 lists the most important retrieval specifics of six NO_2 satellite data sets studied here.

Table 2. Satellite NO_2 slant column density retrievals evaluated in this work.

Retrieval	Fitting window (nm)	Fitting method	Fitted parameters	Wavelength calibration (radiance)	Ref.	Used in
OMNO2A v1	405-465	Intensity fit[a]	NO_2, O_3, H_2O_g[ab], Ring, wavelength shift, polynomial coefficients	Prior to fit 408-423 nm	(1), (2)	DOMINO v2 SP v2
OMNO2A v2	405-465	Intensity fit[a]	NO_2, O_3, H_2O_g[ab], Ring, O_2-O_2, H_2O_{lq}[ab], wavelength shift, polynomial coefficients	Prior to fit 409-428 nm	(2)	~~DOMINO v3~~[b]
OMINO2-QA4ECV	405-465	Optical depth fit[a]	NO_2, O_3, H_2O_g[ab], Ring, O_2-O_2, H_2O_{lq}[ab], I_{off}[c], wavelength shift & stretch, polynomial coefficients	Along with fit 405-465 nm	(3)	QA4ECV OMI
OMNO2-NASA	402-465	Stepwise intensity fit[d]	NO_2, H_2O_g[ab], CHOCHO, Ring, wavelength shift (each micro-window), polynomial	Prior to fit in 7 micro-windows	(4)	SP v3.1[de]

			coefficients (2nd order)			
GONO2A-BIRA	425 - 450	Optical depth fit[f]	NO_2, O_3, O_2-O_2, H_2O_g[~~a~~b], Ring, I_{off}[c], wavelength shift & stretch, polynomial coefficients	Along with fit 420 and 460 nm (5 subwindows)	(2)	TM4NO2A v2.3
GONO2A-QA4ECV[~~e~~g]	405-465	Optical depth fit[f]	NO_2, O_3, O_2-O_2, H_2O_g[~~a~~b], Ring, H_2O_{lq}[~~a~~b], I_{off}[c], wavelength shift & stretch, polynomial coefficients	Along with fit 405-465 nm	(3)	QA4ECV GOME-2A

(1) Bucsela et al., 2006; (2) Van Geffen et al., 2015; (3) QA4ECV Deliverable 4.2~~, 2016~~ [Müller et al., 2016]; (4) Marchenko et al., 2015; this is a reference to the revised spectral fitting algorithm of NO_2 SCDs used in the Standard Product (SP) v3.0 (Krotkov et al., 2017), and which is publicly available at https://disc.gsfc.nasa.gov/datasets/OMNO2_V003/summary/. In our study, we use an updated version (v3.1) (to be released) of OMI NO_2 SCDs and their uncertainties.

[a]Annual average (2005) solar irradiance spectrum is used as reference spectrum.

[~~a~~b]Absorption cross sections of water vapor (H_2O_g) and liquid water (H_2O_{lq}) are used as fitted parameters. The interaction of pure liquid water (e.g. ocean) with incident solar radiation in the VIS (via absorption and vibrational Raman scattering) has an impact on scattered light measured over these areas affecting the DOAS retrievals (Peters et al., 2014).

~~[b]The DOMINO v3 algorithm is not operational yet.~~

[c]The intensity offset, I_{off}, corrects for any additive amount of light (either real, i.e., straylight, or an instrumental artifact, i.e., dark current change) that influences the estimation of the optical depth, $\tau(\lambda) = \ln\left(\frac{I(\lambda)}{I_o(\lambda)}\right)$, with $I(\lambda)$ the earth radiance and $I_0(\lambda)$ the solar irradiance spectrum (Peters et al., 2014).

[d]Monthly averaged solar irradiance spectrum is used as reference spectrum.

[~~d~~e]See Ref. (4)

[f]Daily solar irradiance spectrum is used as reference spectrum.

[~~e~~g]The period 2007-2011 has been processed by IUP Bremen with NLIN software (Richter, A., 1997), and 2012-2015 by BIRA-IASB with QDOAS software (Danckaert et al., 2017) to share the burden of processing tasks. Intercomparison shown that they are very consistent (QA4ECV Deliverable 4.2, section 2.3.1~~, 2016~~ [Müller et al., 2016]).

In the OMNO2A v1 and v2 retrievals, the modelled spectrum is expressed in terms of reflectance (intensity), followed by a non-linear fit to the observed reflectances ("intensity fit"). The modelled reflectance used in OMNO2A v1 and v2 to minimize the fit residual $r(\lambda)$ with the observed $R_{obs}(\lambda)$ is:

$$R_{mod} = \frac{I(\lambda)}{I_0(\lambda)} = P(\lambda) \cdot \exp\left[-\sum_{k=1}^{N_k} \sigma_k(\lambda) \cdot N_{s,k}\right] \cdot \left(1 + C_{Ring} \frac{I_{Ring}(\lambda)}{I_0(\lambda)}\right) + r(\lambda), \tag{1}$$

with $I(\lambda)$ the earth radiance and $I_0(\lambda)$ the 2005 annual average solar irradiance spectrum, and $\sigma_k(\lambda)$ the trace gas cross-sections. The "Ring effect", caused by inelastic Raman scattering of incoming sunlight by N_2 and O_2 molecules (Grainger and Ring, 1962), is accounted for by the term inside the parenthesis on the right hand side of Eq. (1). Here C_{Ring} represents the Ring fitting coefficient and $I_{Ring}(\lambda)/I_0(\lambda)$ the sun-normalised synthetic Ring spectrum. For usage in Eq. (1) σ_k and I_{ring} have been convolved with the instrument slit function. This is different from many other fit models that include the Ring effect as a pseudo-absorber, whereas in OMNO2A it is modelled as a source of photons influencing the backscattered contributions to the modelled reflectance. The radiance I is wavelength calibrated *prior to* solving the above equation, while the irradiance I_0 is assumed to be well-calibrated. All terms in Eq. (1) need to be given at the same wavelength grid; for OMNO2A the irradiance and the reference spectra are interpolated to the (calibrated) radiance wavelength grid. Fit parameters are the trace gas slant columns $N_{s,k}$, the Ring effect coefficient C_{ring}, and the coefficients α_m of the DOAS polynomial $P(\lambda) = \sum \alpha_m \lambda^m$ of order m. Note that Eq. (1) is fully non-linear due to the way the Ring effect is included on the right hand side. OMNO2A v2 slant column retrievals are improved relative to v1 via an optimised window used for the prior-to-fit wavelength calibration, leading to much-reduced fitting errors, and via the inclusion of the absorption by the O_2-O_2 collision complex and by liquid water (H_2O_{lq}) (Van Geffen et al., 2015).

The OMINO2-QA4ECV retrieval performs a χ^2-minimisation of the residual $r(\lambda)$, using the QDOAS software (Danckaert et al., 2017) developed at BIRA-IASB, wherein the modelled spectrum is expressed in terms of optical depth, followed by a mostly linear fit to the observed optical depth (optical depth fit):

$$R^*_{mod} = \ln\left[\frac{I(\lambda') - P_{off}(\lambda')}{I_0(\lambda)}\right] = P^*(\lambda) - \sum_{k=1}^{N_k} \sigma_k(\lambda) \cdot N^*_{s,k} - \sigma_{Ring}(\lambda) \cdot C^*_{Ring} + r^*(\lambda), \tag{2}$$

with $P_{off}(\lambda)$ a 1st order polynomial $P_{off}(\lambda) = c_0 + c_1 \cdot \lambda$ that describes the "intensity offset" correction (denoted as I_{off} in Table 2), and $\lambda' = \lambda_I + \omega_q(\lambda_I - \lambda_0) + \omega_s$ the calibrated radiance wavelength grid, with λ_I the input radiance wavelength grid, ω_s a wavelength shift w.r.t. the wavelength λ_0 of the centre of the fit window and ω_q a stretch ($\omega_q > 0$) or ~~stretch~~ squeeze ($\omega_q < 0$) term. Note that the fit parameters on the left side in Eq. (2), the wavelength calibration and intensity offset correction, constitute non-linear terms in the linear fit. All terms in Eq. (2) need to be given at the same wavelength grid; for QDOAS the calibrated λ' and the reference spectra are interpolated to the irradiance wavelength grid, calibrated before the fit using a high resolution solar spectrum (Fraunhofer calibration). Fit parameters are the trace gas slant columns $N^*_{s,k}$, the Ring effect coefficient C^*_{ring}, the coefficients α^*_m of the DOAS polynomial P^*, the coefficients c_i of the intensity offset polynomial P_{off}, and the wavelength calibration coefficients ω_s and ω_q. The polynomials $P(\lambda)$ and $P^*(\lambda)$ effectively act as the high-pass filter mentioned in the description of the DOAS technique above. The coefficients c_i represent the offset parameter that accounts for instrumental effects like stray-light inside the spectrometer, instrumental thermal instabilities, changes in the detector's dark current, wavelength shifts between I and I_0 or other remaining calibration issues in the level-1 product which are known to be sources of bias in DOAS retrievals of minor trace species. It may also account for atmospheric effects such as incomplete removal of Ring structures (De Smedt et al., 2008; Coburn et al., 2011; Peters et al. 2014; QA4ECV Deliverable 4.2~~, 2016~~ [Müller et al., 2016]).

The χ^2 merit function of the non-linear fit of Eq. (1) is defined by:

$$\chi^2 = \sum_{i=1}^{N_\lambda} \left(\frac{r(\lambda_i)}{\Delta\left(I(\lambda_i)/I_0(\lambda_i)\right)} \right)^2, \tag{3a}$$

with N_λ the number of wavelengths λ_i in the fit interval and $\Delta(I/I_o)$ the standard error on the measurement. In case of the mostly linear fit of Eq. (2) as performed in OMINO2-QA4ECV the residual is not weighted with the error on the measurement, so that the χ^2 merit function is simply given by:

$$\chi^2 = \sum_{i=1}^{N_\lambda} \left(r(\lambda_i) \right)^2, \tag{3b}$$

The magnitude of χ^2 is a measure for how good the fit is. We discuss DOAS SCD uncertainties in more detail in Section 4.1.2.

The OMNO2-NASA algorithm (used in NASA SP v3) uses the intensity fit (Eq. (1)) as default[4], along with monthly-averaged irradiances. The algorithm is different from the OMNO2A and OMINO2-QA4ECV approaches in that it uses a step-by-step (iterative) rather than a simultaneous fitting procedure, wherein a reflectance spectrum is optimized for NO_2 fitting. In the first step, 7 small fitting windows ('micro-windows') are used for iterative wavelength adjustments combined with (window-by-window) removal of the Ring patterns and low-order polynomial smoothing. Wherever appropriate, OMNO2-NASA uses a combination of atmospheric and water-leaving Ring spectra in the $C_{Ring}(\lambda)$ estimates. In this iterative process the irradiances are eventually mapped onto the radiance wavelength grid. Then, in step 2 the NO_2, H_2O and CHOCHO SCDs are sequentially determined in the preliminary spectral regions specifically chosen for the given trace-gas retrieval. After removal of these trace gas absorption features and a thorough evaluation and iterative removal of instrument noise, the final SCDs are obtained via a similar sequential retrieval in slightly adjusted, broad (e.g. 402-465 nm for NO_2) spectral windows optimal for a given trace-gas species.

All four OMI fitting approaches convolve high-resolution absorption cross-section spectra with the OMI slit function (Dirksen et al., 2006; this pre-flight slit function is slightly modified to match the observed irradiances in OMNO2-NASA), which has proved to be stable throughout the OMI mission period (Schenkeveld et al., 2017; Sun et al., 2017). OMNO2A v1

[4]When the intensity fitting approach fails (e.g. yields negative slant columns), the optical depth (Eq. 2) is modelled instead of the reflectances. If optical depth fitting also fails, then the solution from the intensity fit is provided as-is.

uses a fixed slit function for all 60 rows, where in OMNO2A v2 the slit function has been updated w.r.t. OMNO2A v1 to better represent the across-track average (Van Geffen et al. 2015). In the OMINO2-QA4ECV and OMNO2-NASA algorithms, the cross-section spectra have been convolved for each of the 60 across-track positions individually.

3.1.2 GOME-2A NO_2 SCDs

The GONO2A-BIRA spectral fits are performed using the QDOAS software developed at BIRA-IASB, which solves Eq. (2). The GONO2A-BIRA algorithm uses the 425-450 nm window and fits the absorption cross-sections of NO_2, O_3, O_2-O_2 and H_2O_g. The fit also accounts for the Ring effect and includes an intensity offset, along with a 3rd order polynomial. The GONO2A-QA4ECV differs from the GONO2A-BIRA retrieval in the choice of a wider fitting window of 405-465 nm in the retrieval code ~~(NLIN for 2007-2011 and QDOAS for 2012-2015)~~ ~~but~~ and is largely identical to the approach taken in OMINO2-QA4ECV. Both algorithms use daily solar reference spectrum, which contrasts with the use of a fixed annual average or monthly-averaged solar reference spectra in the OMI retrievals. Previous studies indicated that SCDs retrieved from the same sensor in the 405-465 nm window are approximately 0.5×10^{15} molec. cm^{-2} higher than those retrieved from the 425-450 nm window (Van Geffen et al., 2015).

3.2 HCHO slant column density retrievals

Table 3 lists retrieval specifics of the HCHO satellite data sets from OMI and GOME-2A.

Table 3. Satellite HCHO slant column density retrievals evaluated in this work.

Retrieval	Fitting window (nm)	Fitting method	Fitted parameters	Wavelength calibration (radiance)	Ref.
OMIHCHO-BIRA	328.5-346.0	Optical depth fit[a]	HCHO (297 K), O_3 (228 and 243 K), BrO (223 K, pre-fitted[b]), NO_2 (220 K), O_2-O_2 (293 K, pre-fitted[b]), Ring1[c], Ring2[c], O_3L[d], O_3O_3[d], $I_{off,}$ wavelength shift, polynomial coefficients	Along with fit 325-360 nm (5 subwindows)	(1)
OMIHCHO-QA4ECV	328.5-359.0	Optical depth fit[e]	HCHO, O_3 (223 and 243 K), BrO, NO_2, O_2-O_2, Ring, O_3L[d], O_3O_3[d], $I_{off,}$ wavelength shift &	Along with fit 325-360 nm	(2)

			stretch, polynomial coefficients		
GO2AHCHO-BIRA	328.5–346.0	Optical depth fit[a]	HCHO (297 K), O_3 (228 and 243 K), BrO (223 K, pre-fitted[b]), NO_2 (220 K), O_2-O_2 (293 K, pre-fitted[b]), Ring1[c], Ring2[c], O_3L[d], O_3O_3[d], I_{off}, Eta and zeta polarization vectors, wavelength shift & stretch, polynomial coefficients	Along with fit 325-360 nm (5 subwindows)	(1)
GO2AHCHO-QA4ECV	328.5-359.0	Optical depth fit[e]	HCHO, O_3 (223 and 243 K), BrO, NO_2, O_2-O_2, Ring, O_3L[d], O_3O_3[d], I_{off}, Eta and zeta polarization vectors, pseudo cross-section to correct for East-West bias, wavelength shift & stretch, polynomial coefficients	Along with fit 325-360 nm	(2)

(1) De Smedt et al., 2015; (2) QA4ECV Deliverable 4.2~~, 2016~~ [Müller et al., 2016]

[a]Instead of a solar irradiance spectrum, daily Earth radiance spectra over the Equatorial Pacific (15°S–15°N, 180–240°E) are used as reference spectrum.

[b]BrO and O_4 are pre-fitted in the 328.5–359 nm and 339–364 nm wavelength intervals, respectively. The resulting SCD in each case is used as a fixed value in the nominal window of 328.5-346.0 nm.

[c]Two cross sections are used to account for the Ring effect (Vountas et al., 1998), calculated in an ozone-containing atmosphere for low and high SZA (solar zenith angle) using LIDORT RRS (Spurr et al., 2008).

[d]Two additional terms (O_3L and O_3O_3) are included to better cope with strong O_3 absorption effects (Puķīte et al., 2010; De Smedt et al., 2012). They result from the Taylor expansion of the O_3 absorption as a function of the wavelength.

[e]Instead of a solar irradiance spectrum, daily Earth radiance spectra over the Equatorial Pacific (15°S–15°N, 150–250°E) are used as reference spectrum.

For OMI and GOME-2 HCHO retrievals, a dynamical convolution of the cross-sections is performed along with the fit using the improved slit function derived prior to the fit, during the Fraunhofer calibration. The QA4ECV HCHO retrievals share many aspects with the QA4ECV spectral fitting for NO_2. QA4ECV and BIRA HCHO SCD retrievals are also very similar in absorption cross-sections and retrieval code used (QDOAS, solving Eq. (2)). The most prominent differences between the QA4ECV and BIRA retrievals are the following:

1. ~~The f~~Fitting windows: while the BIRA retrievals used a reduced fitting interval (328.5-346 nm), combined with pre-fits of O_{2}~~$_{4}$~~$-O_2$ and BrO slant columns in dedicated windows, the QA4ECV retrievals use one single extended fitting interval (328.5-359 nm). There is therefore no pre-fit of O~~$_{4}$~~$_{2}-O_2$ and BrO slant columns in QA4ECV. However the switch to an extended fitting interval introduces additional retrieval difficulties for GOME-2, since this instrument suffers from polarization structures not fully corrected by level 0-1 processing leading to scan-angle depend biases in HCHO. To mitigate these biases, polarization response cross-sections (eta and zeta) are added to the fit together with an empirical cross-section derived from E/W mean fitting residuals (Richter et al., EGU General Assembly, 2016). While successful in eliminating polarization-related biases, these additional cross-sections have a non-negligible impact on the retrieval noise and its time evolution (this issue is further illustrated in sections 4.1.5 and 4.3.3).
2. Different Ring corrections are used: ~~(~~change from Vountas et al. [1998] to Chance and Spurr [1997] spectrum~~)~~.
3. An ~~I~~improved earthshine reference selection scheme is implemented ~~wavelength calibration for QA4ECV (shift & stretch on solar spectrum)~~ for GOME-2~~;~~: Earth radiance ~~radiance~~ spectra are now grouped along viewing zenith angle instead of one generic Earth radiance reference spectrum. ~~and a pseudo cross-section is used to account for E/W bias in the extended fitting interval (Richter et al., EGU General Assembly, 2016).~~

4 Results and Discussion

4.1 Quality assessment of NO_2 and HCHO slant column densities

4.1.1. Slant column density intercomparisons

We compare the NO_2 SCDs from the OMNO2A v2, OMNO2-NASA and OMINO2-QA4ECV algorithms, against OMNO2A v1. Figure 1 (left panel) shows average absolute NO_2 SCDs as a function of latitude for all four OMI SCD products for unpolluted Pacific orbits from day 1 of January, April, July and October 2005 up to 2015. The SCDs show lowest values in the Tropics (shorter light path and lower VCDs), and higher values poleward. Averaged over all latitudes, the revised algorithms result in 12-15% lower SCDs ($1.2\text{-}1.4\times10^{15}$ molec. cm^{-2}) than OMNO2A v1 SCDs, in line with the reductions reported for OMNO2A v2 in Van Geffen et al. [2015]. The revised OMNO2A v2, OMINO2-QA4ECV and OMNO2-NASA SCDs are in close agreement (differences <4%). The OMNO2-NASA SCDs (and their uncertainties) used in this analysis correspond to the latest version (v3.1; to be released) of the new Standard Product (SP) (Krotkov et al. [2017]). Over the chosen clean-sector area the v3.1 SCDs are on average higher by ~0.5×10^{15} molec. cm^{-2} than v3.0. Differences between v3.1 and v3.0 SCD values are related to the changed approach to flagging of the presumably noisy wavelength bins in the OMI radiances, as well as improved solar reference spectra.The GOME-2A NO_2 SCDs (Figure 1;

right panel) are ~2-3×10^{15} molec.cm^{-2} lower than OMI's, which is anticipated because of the diurnal increase in stratospheric NO_2 (e.g. Dirksen et al., 2011) and differences in ~~solar zenith angles~~ viewing geometries. The GONO2A-QA4ECV SCDs are in line with GONO2A-BIRA, with the latter showing on average slightly lower values (by <0.5×10^{15} molec.cm^{-2}), reflecting the similarity of the BIRA and QA4ECV algorithms. Their main differences are the choice of fitting window and that the H_2O_{lq} is not fitted in the small fitting window (for GONO2A-BIRA). Their relative difference is highest (~12%) around the Equator.

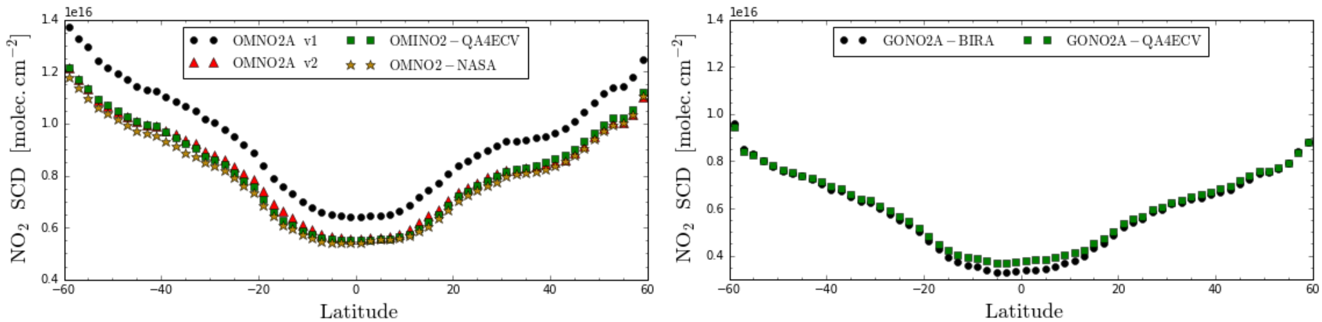

Figure 1. Average NO_2 slant columns within 2°-wide latitudinal bins for OMNO2A v1 (black circles), OMNO2A v2 (red triangles), OMINO2-QA4ECV (green squares) and OMNO2-NASA (yellow stars) algorithms (left panel), and for GONO2A-BIRA (black circles) and GONO2A-QA4ECV (green squares) algorithms (right panel) for the Pacific (reference sector: 60°N-60°S and 150°-180°W) orbit from day 1 of January, April, July and October (or closest available data) 2005-2015 for OMI and 2007-2015 for GOME-2A.

For HCHO, a comparison of SCDs is less straightforward than for NO_2. First of all, daily Earth radiance spectra are used as a reference for the DOAS retrievals instead of solar irradiance spectra. The Earth radiance reference spectra are taken over a reference sector in the Equatorial Pacific, where CH_4 oxidation is the only significant source of HCHO. The resulting (differential) HCHO SCD may then have values close to zero, or even be negative, indicating that a scene has a similar or smaller HCHO amount than in the reference spectrum. After the fit, a background correction is applied on the SCDs (De Smedt et al., 2015). The final differential SCDs (ΔSCDs) are the result of subtracting the mean HCHO SCD over each OMI row and by 5° of latitude bins within the reference sector (N_{s0}), from the SCDs (N_s) of the same day, $\Delta N_s = N_s - N_{s0}$ (QA4ECV Deliverable 4.2~~, 2016~~ [Müller et al., 2016]; ~~S5P/TROPOMI HCHO ATBD, 2016;~~ De Smedt et al., 2017; De Smedt et al., 2018). This normalisation approach and the choice of daily radiance spectra result in ΔSCDs close to zero over the reference region. Selecting daily Earth radiance reference spectra helps to reduce the effects of radiance degradation for GOME-2A retrievals, and the effects of stripes for OMI. The final tropospheric HCHO vertical columns (N_v) are then defined as $N_v = \frac{\Delta N_s}{M} + \frac{M_0}{M} N_{v,0,CTM}$; where M is the tropospheric AMF, and M_0 and $N_{v,0,CTM}$ are respectively the AMF and the model background column in the reference sector.

Figure 2 (left panel) shows a comparison of HCHO SCDs before (light lines) and after (dark lines) background correction from the OMIHCHO-QA4ECV and OMIHCHO-BIRA algorithms. Their differential SCDs (ΔSCDs; green and black symbols) are highly consistent with only a small difference of ~0.7×10^{15} molec. cm^{-2}, on average. This suggests that the improvements made in the QA4ECV OMI HCHO fitting code do not lead to substantial changes in the HCHO columns, but we will see later that there is considerable impact on the uncertainties of the fits.

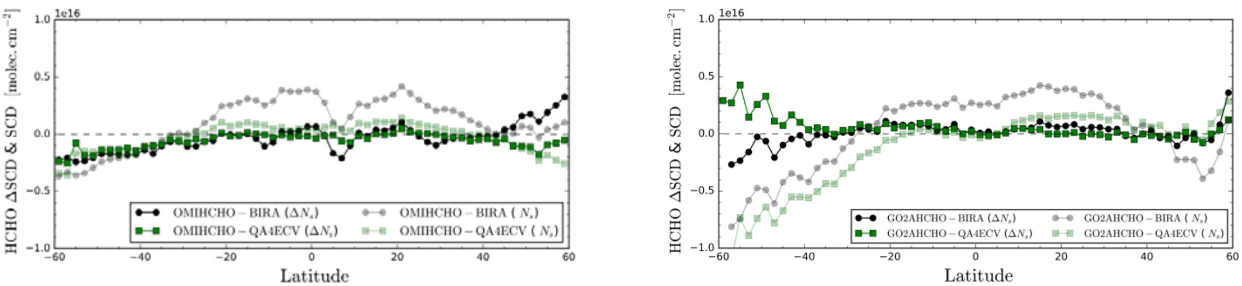

Figure 2. Average differential HCHO slant columns within 2°-wide latitudinal bins for (left panel) OMIHCHO-BIRA (black circles) and OMIHCHO-QA4ECV (green squares) for the Pacific (60°N-60°S and 150°-180°W) orbit from day 1 of January, April, July and October (or closest available data) 2005-2015, and for (right panel) GO2AHCHO-BIRA (black circles) and GO2AHCHO-QA4ECV (green squares) for the Pacific orbits from day 1 of January up to December and from day 15 of January, April, July and October (or closest available data) 2007-June 2014 and 2007-2015, respectively. The light grey and green lines represent the HCHO SCDs before the background correction.

We see similar behaviour for the GOME-2A HCHO SCDs provided by the GO2AHCHO-BIRA and GO2AHCHO-QA4ECV algorithms (Figure 2; right panel). As with OMI, averaged over all latitudes the difference between ΔSCDs is small (<0.9×10^{15} molec. cm^{-2}). For the retrieved SCDs, the differences are larger (up to 15×10^{15} molec. cm^{-2}) at all latitudes, stressing the importance of the background correction.

4.1.2 Evaluating slant column density uncertainties

4.1.2.1 DOAS SCD uncertainty

The DOAS technique tries to minimize the differences between the observed and the modelled spectra within a nominal wavelength window (spectral points of length *K*). The Levenberg-Marquardt non-linear least-squares fitting procedure (M-L) is the numerical routine that performs the χ^2 –merit function minimisation (Press et al., 1997) and provides the fitting parameters (of length *M*) (SCDs, N_s) and a covariance matrix that contains an estimate of the uncertainty in the fitting parameters (SCD uncertainty, $\varepsilon_{N_{s,j}}$; "DOAS SCD uncertainty" hereafter) for a typical non-linear fit. This routine is also used by a mostly linear fit in order to find the non-linear parameters, followed by a solution (the QR decomposition of the cross-sections matrix for QDOAS and the singular value decomposition for NLIN) for a typical least squares problem for the linear parameters.

The diagonal elements of the covariance matrix, [C], are the variances of the fitted parameters. The uncertainty in the fitted parameter, $\varepsilon_{N_{s,j}}$, is the square root of the variance:

$$\varepsilon_{N_{s,j}} = \sqrt{\chi^2 \left(A^T A\right)^{-1}_{jj}} \tag{4}$$

where **A** is the matrix formed by the absorption cross-sections whose $K \times M$ components are constructed from the M basis functions evaluated at the K abscissas x_i (i.e. $X_1(x)$, …, $X_M(x)$), and from the K measurement errors ε_i, by the prescription

$$A_{ij} = \frac{X_j(x_i)}{\varepsilon_i} \qquad \begin{array}{l} , i = 1, \ldots, K \\ j = 1, \ldots, M \end{array}$$

The off-diagonal elements are the covariances between the parameters. In the non-linear intensity fit approach of Eq. (1) all components of the fit are accounted for in the uncertainty estimate. In the QDOAS- and NLIN- fit (Eq. (2)) only the linear components in the fit are accounted for: uncertainties on estimated values of the non-linear parameters (i.e. shift, squeeze and intensity offset parameters) are not taken into account in the uncertainty estimate of the SCDs (QDOAS Software user manual, version 3.2, 2017) and the measurement errors are not used in the fit ($\varepsilon_i = 1$). The SCD uncertainties are then estimated using the reduced χ^2 (instead of the nominal χ^2), i.e. Eq. (3b) divided by the number of degrees of freedom in the fit, K-M.

Uncertainties on the retrieved SCDs thus depend on:

1. the accuracy (sensitivity) of the fitting model in capturing the ensemble of spectral features in the observed, noisy reflectance spectrum,
2. the uncertainty in the measurements,
3. wavelength calibration.

The DOAS SCD uncertainty may consist of two parts: a random and a systematic error component.

4.1.2.2 *A posteriori* statistical SCD uncertainty

To evaluate the DOAS SCD uncertainty estimates and to have an independent means to inter-compare the results of the different retrieval methods, we apply an alternative, statistical method. We follow the approach laid out in Wenig et al. [2001] and Boersma et al. [2007], to quantify the spatial SCD variability over pristine, unpolluted areas and assume that such estimates serve as a statistical indicator of the SCD uncertainty. The main contributors to the SCD variability are the instrument (level-1) noise, natural variability within the unpolluted area, scene reflectance (surface, clouds) and viewing geometry variability. Our objective is to provide an estimate of the random component of the SCD uncertainty by limiting the contributions from other components to the variability over the unpolluted area. We focus our analysis on the remote area within 60°N-60°S and 150°-180°W (Pacific Ocean). Practically free of tropospheric pollution, this area is separated in 2°×2° (longitude × latitude) "boxes", which limits geophysical variability and provides statistically robust sampling. We assume that pixels within each box record the same NO_2 or HCHO total vertical columns. Any variability emerging in the retrieved (all- or clear-sky) ensemble is then attributed to random uncertainty originating from noise in the level 1 data and imperfections in the spectral fitting model, as long as the geometric AMFs within the box show little variability[5]. Sun glint over the ocean may cause natural SCD variability for mostly cloud-free scenes, and we investigate this further by segregating the data into two broad categories.

Boxes with relative AMF variability of more than 5% are discarded, to prevent variability in viewing geometry influencing the results. In practice, the AMF variability in most boxes does not exceed 3.5%, i.e. SCDs in each box are observed under very similar viewing geometries. For these boxes we compute standard deviations of the SCDs as the statistical SCD uncertainties. In the DOAS-fit, NO_2 is fitted assuming a fixed temperature for its absorption cross section of T_0 = 220 K and HCHO is fitted assuming T_0 = 298 K. In most retrieval algorithms, a post-correction on the slant columns is applied to compensate for neglecting the actual atmospheric temperature of the trace gas, but this is typically done in the later AMF step. The slant columns used in this analysis are not yet corrected for the temperature-dependency of the NO_2 and HCHO absorption cross-sections. For all OMI algorithms the DOAS uncertainty estimates may contain contributions from stripes. The statistical HCHO SCD uncertainties reported in the following sections concern the differential HCHO SCDs (ΔSCDs), which are known to suffer to a lesser exten~~d~~t from this artefact (see Sections 2.1 and 4.3).

4.1.3 OMI NO_2 SCD uncertainties

We now compare the OMI NO_2 DOAS and statistical SCD uncertainty estimates. ~~The OMNO2-NASA SCDs and uncertainties used in this analysis correspond to the latest (v3.1, to be released by the end of 2017) version of the new Standard Product (Krotkov et al. [2017]: initial v3.0 released in 2016). Over the chosen clean-sector area the v3.1 SCDs are on average higher by ~0.5×10^15 molec. cm^-2 than v3.0, and the v3.1 DOAS SCD uncertainties 40% lower than in v3.0. We find that the statistical SCD uncertainties are similar between v3.1 and v3.0 (agreement within 0.02×10^15 molec. cm^-2).~~
The algorithms show a slight decrease of statistical and DOAS NO_2 SCD uncertainties with increasing latitude (Figure 3). For OMNO2A v1, v2, and OMINO2-QA4ECV the DOAS uncertainty exceeds the statistical uncertainty. We attribute this to

[5]The relative AMF variability for each box was computed as follows: $\left(\overline{M_i^2} - \overline{M_i}^2\right)^{0.5} \Big/ \overline{M_i}$, where M_i is the AMF attributed to each pixel within the box.

persistent (systematic) fitting residuals, and signatures unexplained by the fitting technique. Averaged over all latitudes, the relative difference between the statistical and DOAS uncertainty reduces from ~60% for OMNO2A v1 to ~20% for OMINO2-QA4ECV. This reduction hints at an improved understanding of the spectral features, and especially the reduction of systematic parts of the residuals in the OMINO2-QA4ECV spectral fitting method relative to OMNO2A v1, in line with findings in Van Geffen et al. [2015] and Anand et al. [2015] that OMNO2A v1 was suffering from inaccurate wavelength calibration.

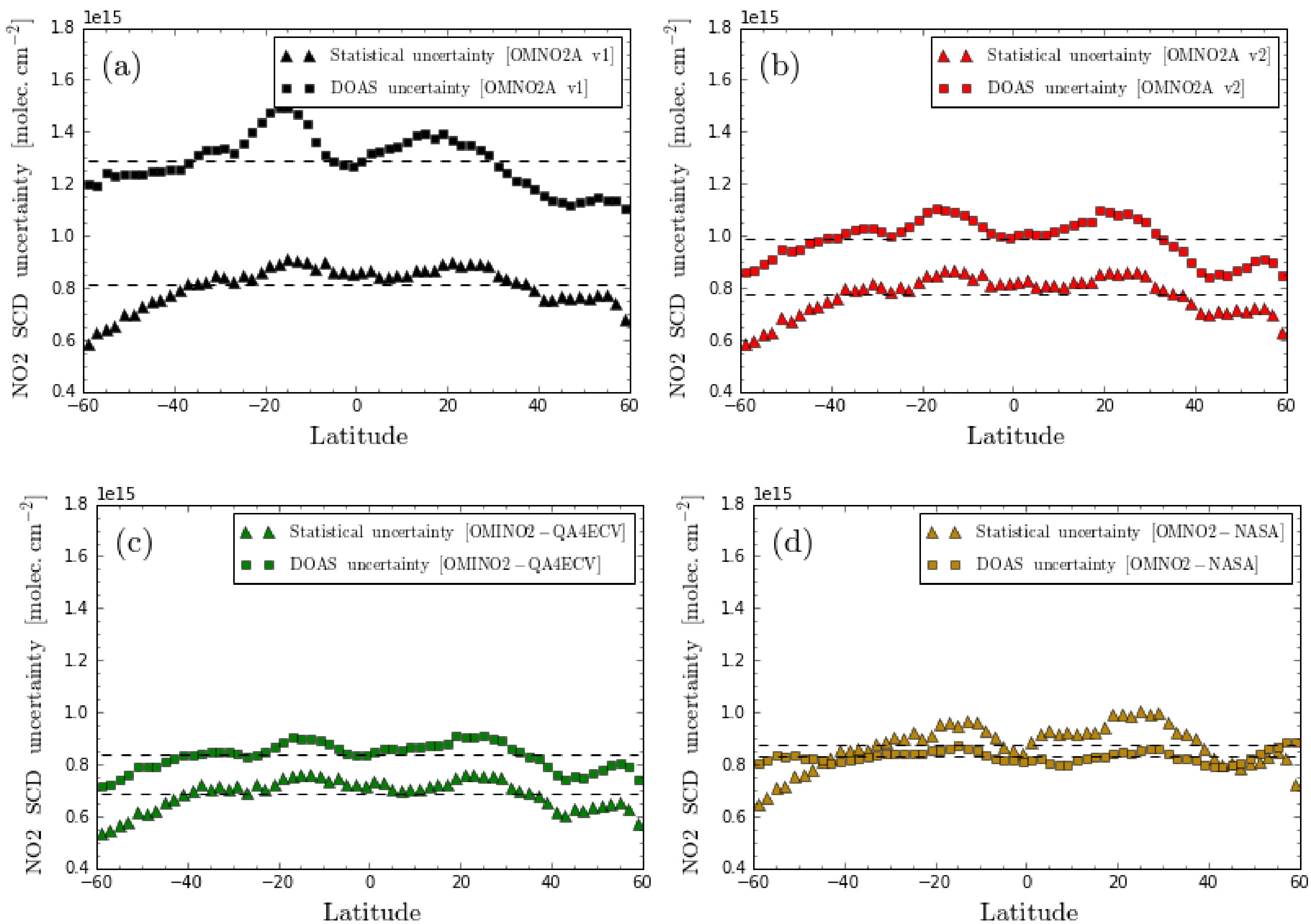

Figure 3. Average statistical (triangles) and DOAS (squares) OMI NO_2 SCD uncertainty of all boxes within 2^o-wide latitudinal bins for the OMNO2A v1 ((a) black), OMNO2A v2 ((b) red), OMINO2-QA4ECV ((c) green) and OMNO2-NASA ((d) yellow) slant columns for the Pacific orbit from day 1 of January, April, July and October 2005-2015. The standard deviation of the slant columns in a box stands for the statistical uncertainty while the box-mean value of the DOAS-fit uncertainties stands for the DOAS uncertainty. We require at least 10 pixels within a box for a robust application of statistical analysis. The dashed line represents the average slant column uncertainty over all latitudes. No cloud-screening has been applied.

Both statistical and DOAS SCD uncertainties are on average smallest for OMINO2-QA4ECV (15% and 35% lower than OMNO2A v1), which may indicate~~s~~ a more physically accurate fitting model for that algorithm. The DOAS uncertainty from OMNO2-NASA shows a smoother geographical variation than the pattern of the statistical uncertainty, which shows substantial variation with latitude (Figure 3d). The OMNO2-NASA DOAS and statistical uncertainty are of similar magnitude, in contrast to higher DOAS than statistical uncertainties for OMNO2A v1, v2 and OMINO2-QA4ECV. The OMNO2-NASA v3.1 DOAS SCD uncertainties are on average 40% lower than v3.0. This reduction of the DOAS SCD uncertainties stems from correction of an error in the v3.0 algorithm. The statistical SCD uncertainties are similar between v3.1 and v3.0 (agreement within 0.02×10^{15} molec. cm^{-2}). The DOAS and statistical uncertainties shown in Figure 3 for the OMNO2A versions are consistent with estimates reported for OMNO2A v1 in Boersma et al. [2007] and Anand et al. [2015], and for OMNO2A v~~1~~2~~,~~ ~~and~~ in Van Geffen et al. [2015]~~. for OMNO2A v2~~.

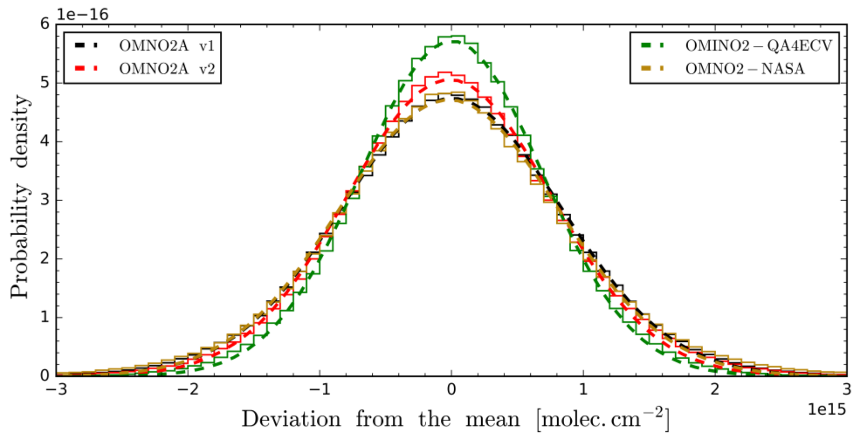

Figure 4. Distribution of the deviation of the OMI NO_2 SCDs from the mean-SCD within a box (for all boxes) in a histogram for OMNO2A v2 (red), OMINO2-QA4ECV (green) and OMNO2-NASA (yellow) algorithms against the reference OMNO2A v1 (black). The width, σ, of the Gaussian provides an estimate of the SCD uncertainty for each SCD retrieval algorithm ($\sigma_{v1} = 0.833\pm0.003\times10^{15}$ molec. cm^{-2}, $\sigma_{v2} = 0.776\pm0.005\times10^{15}$ molec. cm^{-2}, $\sigma_{qa4ecv} = 0.688\pm0.003\times10^{15}$ molec. cm^{-2}, $\sigma_{nasa} = 0.829\pm0.006\times10^{15}$ molec. cm^{-2}). The histogram contains contributions from all boxes within the reference sector for the Pacific orbit from day 1 of January, April, July and October 2005-2015. No cloud-screening has been applied.

Figure 4 shows histograms of the absolute differences between the individual SCDs and the box-mean SCD for OMNO2A v1 and v2, OMINO2-QA4ECV, and OMNO2-NASA. The histogram of SCD differences in the OMINO2-QA4ECV ensemble has the highest peak and smallest width (FWHM 1.6×10^{15} molec. cm^{-2}) of the four algorithms. All histograms closely follow a Gaussian distribution, which is consistent with our initial assumption that random errors in the slant columns are responsible for the variability within each box, and originate mostly from measurement noise. The width (1σ) of the Gaussian function fitted to the observed distributions can be used as an alternative indicator of the overall, mission-averaged statistical uncertainty in the SCDs for the different algorithms. The mission-average uncertainty for the OMINO2-

QA4ECV amounts to 0.69×10^{15} molec. cm^{-2}, with significantly larger values for the OMNO2A and OMNO2-NASA algorithms. ~~In Section 4.2 we will see that the OMINO2-QA4ECV DOAS SCD uncertainties are improved relative to OMNO2A v1 on a global scale; they appear significantly lower and free of high viewing or solar zenith angle dependencies.~~ These findings are in agreement with the statistical uncertainty averaged over all latitudes shown as dashed lines in Figure 3. Table 4 summarizes the estimates of the statistical and DOAS uncertainties for OMNO2A v1, v2, OMINO2-QA4ECV and OMNO2-NASA SCDs for all-sky and clear-sky situations.

Table 4. Statistical and DOAS uncertainty estimates of OMI NO_2 SCDs for OMNO2A v1, v2, OMINO2-QA4ECV and OMNO2-NASA algorithms, and of GOME-2A NO_2 SCDs for GONO2A-BIRA and GONO2A-QA4ECV algorithms, for the Pacific orbit from day 1 of January, April, July and October 2005-2015 for all-sky conditions (top panel) and clear-sky conditions (cloud radiance fraction <0.5) (bottom panel). The cloud radiance fraction (crf) is the fraction of the radiation from the cloudy part of the pixel.

SCD uncertainty (all-sky)	OMNO2A v1 [molec. cm^{-2}]	OMNO2A v2 [molec. cm^{-2}]	OMINO2-QA4ECV [molec. cm^{-2}]	OMNO2-NASA [molec. cm^{-2}]	GONO2A-BIRA [molec. cm^{-2}]	GONO2A-QA4ECV [molec. cm^{-2}]
Statistical	0.83×10^{15}	0.78×10^{15}	0.69×10^{15}	0.83×10^{15}	0.64×10^{15}	0.56×10^{15}
DOAS	1.32×10^{15}	0.99×10^{15}	0.84×10^{15}	0.83×10^{15}	0.89×10^{15}	0.80×10^{15}
SCD uncertainty (crf < 0.5)						
Statistical	0.89×10^{15}	0.85×10^{15}	0.76×10^{15}	0.89×10^{15}	0.94×10^{15}	0.73×10^{15}
DOAS	$1.36 \times\cdot 10^{15}$	1.11×10^{15}	0.91×10^{15}	0.89×10^{15}	$1.15\times\cdot 10^{15}$	0.94×10^{15}

One question is whether SCDs for dark scenes are more uncertain than the SCDs obtained for bright scenes. The dark scenes, often associated with clear-sky conditions (cloud radiance fraction <0.5), are of most interest for tropospheric retrievals. In the studies by Anand et al. [2015] and Marchenko et al. [2015], it was suggested that spectral fitting over (partly) cloudy scenes may result in less stable SCDs because of substantial wavelength-shifts caused by the inhomogeneous illumination of the instrument slit (Voors et al., 2006). On the other hand, bright scenes have higher reflectance levels, and therefore potentially higher signal-to-noise ratios, and if the wavelength calibration is sufficiently accurate in the fitting procedure, lower SCD uncertainties may be expected for such scenes. We repeated the statistical tests for the spectral fitting algorithms shown in Figures 3 and 4, but now selected only SCDs obtained under relatively cloud-free (‘clear-sky’ for brevity) conditions. For clear-sky scenes, the SCD uncertainty varies less with latitude than shown in Figure 3 and the absolute uncertainties are higher by a factor of 1.1 compared to the all-sky SCD uncertainty estimates. This indicates that reduced signal-to-noise in the level-1 data (dark scenes) increases absolute SCD uncertainties. We recommend using the statistical estimates for clear-sky conditions in Table 4 as adequate estimates of SCD uncertainties for the above algorithms in the context of tropospheric NO_2 column retrievals.

Boersma et al. [2007] reported that the uncertainty in the OMI NO_2 retrievals due to spectral fitting with the OMNO2A v1 setup is of the order of 0.7×10^{15} molec. cm^{-2} based on the variability seen in the de-striped SCDs over the Pacific on 7 August 2006, when the row anomaly was still confined and affected only one of OMI's rows. The larger statistical uncertainty found here for the OMNO2A v1 SCDs for the 2005-2015 time period (~0.8×10^{15} molec. cm^{-2}) is thus reasonable. The OMNO2A v2 statistical uncertainty is slightly (~6%) lower than for OMNO2A v1. Van Geffen et al. [2015] found the DOAS SCD uncertainties computed by the OMNO2A v1 and v2 spectral fits to be approximately 1.3×10^{15} molec. cm^{-2} and 1.0×10^{15} molec. cm^{-2}, respectively, for Pacific Ocean orbits in 2007. The improvements to the OMNO2A v2 spectral fit reduced the DOAS slant column uncertainty by approximately 0.3×10^{15} molec. cm^{-2} (or 24%). The results from our 11-year period investigated here are consistent with those findings (Table 4).

4.1.4 GOME-2A NO_2 SCD uncertainties

Here we compare the GONO2A-QA4ECV against GONO2A-BIRA SCD uncertainties (Figure 5 and Table 4). As with OMI, the GOME-2A NO_2 DOAS uncertainties exceed the statistical ones. Averaged over all latitudes (not shown), for GONO2A-BIRA the DOAS uncertainty exceeds the statistical uncertainty by 26%, and by 35% for GONO2A-QA4ECV. The improvement in GONO2A-QA4ECV spectral fitting is demonstrated by both DOAS and statistical uncertainties being on average 10% and 13% smaller than those for the GONO2A-BIRA dataset. This is confirmed by Figure 5c, which shows the highest peak and smallest width in the histogram of the SCD vs. box-mean SCD differences for GONO2A-QA4ECV (FWHM 1.3×10^{15} molec. cm^{-2}) compared to GONO2A-BIRA (FWHM 1.5×10^{15} molec. cm^{-2}). The deviations of the SCDs from the box-mean SCD form a normal distribution illustrative of the random nature of the noise in the GOME-2A level-1 data which drives the total SCD uncertainty. We conclude that, similar to OMI, the improved QA4ECV fitting algorithm results in more precise fitting results for NO_2.

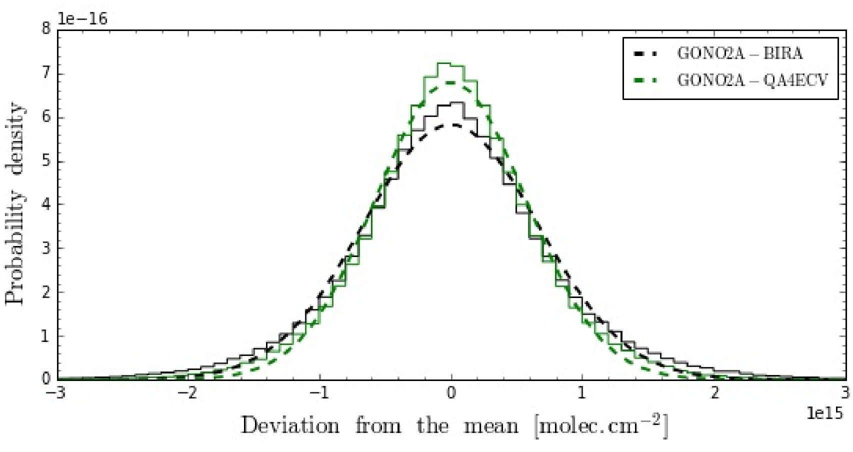

Figure 5 ~~(a), (b) Average statistical (triangles) and DOAS (squares) GOME-2A NO_2 SCD uncertainty of all boxes within 2° wide latitudinal bins for the GONO2A-BIRA (black) and GONO2A-QA4ECV (green) slant columns for the Pacific orbit from day 1 of January, April, July and October 2007-2015. The statistical and DOAS uncertainties are defined similarly to Figure 3. (c)~~ Distribution of the deviation of the SCDs from the mean-SCD within a box (for all boxes) in a histogram for GONO2A-QA4ECV (green) algorithm against the reference GONO2A-BIRA (black). The width, σ, of the Gaussian provides an estimate of the SCD uncertainty for each SCD retrieval algorithm ($\sigma_{bira} = 0.635 \pm 0.008 \times 10^{15}$ molec. cm^{-2}, $\sigma_{qa4ecv} = 0.556 \pm 0.006 \times 10^{15}$ molec. cm^{-2}). The histogram contains contributions from all boxes within the reference sector for the Pacific orbit from day 1 of January, April, July and October 2007-2015. No cloud-screening has been applied.

Note: Former Figures 5(a) and (b) are now removed. The former Figure 5(c) is now the new Figure 5.

The mission-average QA4ECV NO_2 SCD uncertainties from OMI and GOME-2A are comparable in magnitude; the statistical and DOAS uncertainty for GOME-2A (0.56×10^{15} molec. cm^{-2} and 0.80×10^{15} molec. cm^{-2}) are lower than for OMI (0.69×10^{15} molec. cm^{-2} and 0.84×10^{15} molec. cm^{-2}). Initially, ~~one may expect much~~a higher spectral fit quality was expected for GOME-2A, because of the instrument's higher signal-to-noise (2× larger than OMI; see Table 1). This is indeed the case for the early years of the instruments' mission. In 2007, the GOME-2A NO_2 SCD statistical uncertainty ($\sim 0.45 \times 10^{15}$ molec. cm^{-2}; Figure 11(left)) was lower than for OMI ($\sim 0.66 \times 10^{15}$ molec. cm^{-2}; Figure 9(c)). ~~We see here that this is not quite the case, probably due to t~~The relatively fast degradation of the GOME-2A level-1 data has deteriorated the quality of the GOME-2A fits as diagnosed by: (1) severe throughput loss (see Section 2.2), (2) instability of the instrument slit function due to thermal fluctuations of the GOME-2A optical bench, and (3) potential degradation of the reflectance. In contrast, OMI has shown exceptional stability, even after the occurrence and expansion of the row anomaly, and after exceeding its designed lifespan by far. This explains why GOME-2A retrievals show comparable SCD uncertainties to OMI's and will be discussed in detail in Section 3.

4.1.5 OMI and GOME-2A HCHO SCD uncertainties

The spectral fitting of HCHO is more challenging than for NO_2~~. Even with pronounced absorption signatures and relatively large abundance in the atmosphere (of the order of 10×10^{15} molec. cm^{-2}), the fitting of the HCHO SCDs in earth radiances is difficult~~ because of its relatively small differential optical depth (~~typically one order of magnitude smaller than NO_2; see~~ Table 1), lower instrument signal-to-noise in the UV and stronger interferences from other absorbing species (e.g. from O_3). Therefore, measurement noise and the presence of other species' absorption fingerprints in the same fitting window limit the HCHO detection. This is reflected by the larger random (and systematic) SCD uncertainties for HCHO relative to NO_2. The OMIHCHO-QA4ECV SCDs have an uncertainty of $\sim 8 \times 10^{15}$ molec. cm^{-2} (Figure 6a), 10 times larger than OMINO2-QA4ECV (~~$\sim 0.8 \times 10^{15}$ molec. cm^{-2},~~ Table 4). As for NO_2, QA4ECV results also show smaller OMI HCHO SCD uncertainties compared to the BIRA algorithm. The wider QA4ECV fitting window allows the reduction of the SCD uncertainty even though bromine monoxide (BrO) is now included in the fitting procedure (and not pre-fitted). On average, the OMIHCHO-

QA4ECV SCD uncertainties are 18% smaller than those from OMIHCHO-BIRA, confirming the improvements in spectral fitting, consistent with the extensive tests and improvements for OMI HCHO fitting (QA4ECV Deliverable 4.2~~, 2016~~ [Müller et al., 2016]).

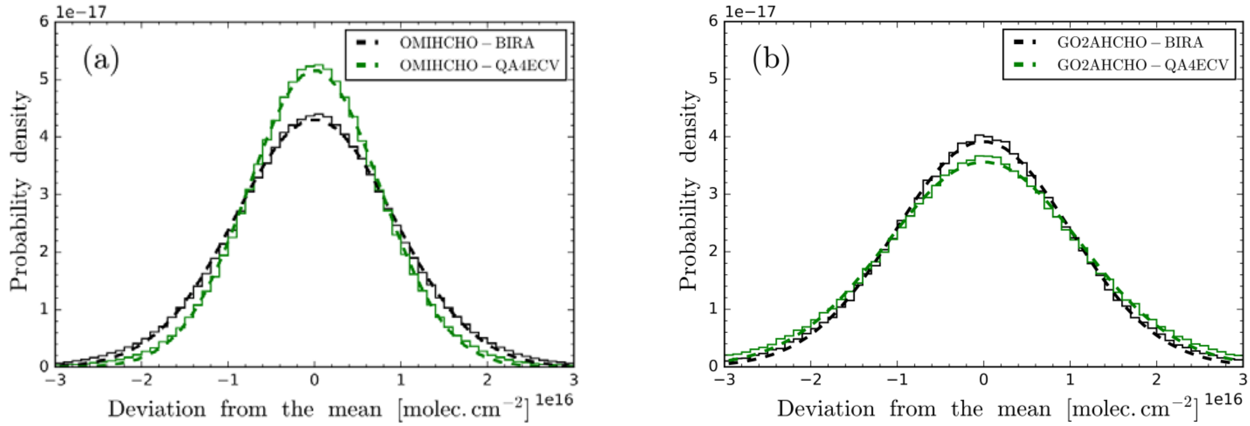

Figure 6 (a) Distribution of the deviation of the SCDs from the mean-SCD within a box (for all boxes) in a histogram for OMIHCHO-QA4ECV (green) against the reference OMIHCHO-BIRA (black) for the Pacific orbit from day 1 of January, April, July and October 2005-2015. The width, σ, of the Gaussian provides an estimate of the SCD uncertainty for each SCD retrieval algorithm ($\sigma_{bira} =$ 9.10±0.04×10^{15} molec. cm^{-2}, $\sigma_{qa4ecv} =$ 7.55±0.04×10^{15} molec. cm^{-2}). (b) as (a) but for GO2AHCHO-BIRA and GO2AHCHO-QA4ECV the Pacific orbits from day 1 of January up to December and from day 15 of January, April, July and October 2007-June 2014 and 2007-2015, respectively, were used ($\sigma_{bira} =$ 10.11±0.06×10^{15} molec. cm^{-2}, $\sigma_{qa4ecv} =$ 11.17±0.07×10^{15} molec. cm^{-2}).

The new GOME-2A fitting algorithm (GO2AHCHO-QA4ECV) did~~oes~~ not result in statistically significant reduction of SCD uncertainties compared to the BIRA algorithm (Figure 6b and Table 5). On average, the HCHO statistical SCD uncertainty for GO2AHCHO-QA4ECV is 11% higher than for GO2AHCHO-BIRA. The apparent lack of improvement is discussed in Section 4.3.3.

Table 5. Statistical and DOAS uncertainty estimates of OMI and GOME-2A HCHO SCDs for OMIHCHO-BIRA and OMIHCHO-QA4ECV (Pacific orbit from day 1 of January, April, July and October (or closest available data) 2005-2015), and GO2AHCHO-BIRA and GO2AHCHO-QA4ECV (Pacific orbit from day 1 of January up to December and from day 15 of January, April, July and October (or closest available data) 2007-June 2014 and 2007-2015, respectively) for all-sky conditions (top panel) and clear-sky conditions (bottom panel). The GO2AHCHO-BIRA data are provided only for scenes with cloud fraction lower than 0.4, therefore the clear-sky conditions yield similar SCD uncertainties to the all-sky conditions. Cloud radiance fraction values are typically larger than cloud fraction values therefore SCD uncertainties for clear-sky conditions are still slightly larger than the all-sky ones.

SCD uncertainty (all-sky)	OMIHCHO-BIRA [molec. cm^{-2}]	OMIHCHO-QA4ECV [molec. cm^{-2}]	GO2AHCHO-BIRA [molec. cm^{-2}]	GO2AHCHO-QA4ECV [molec. cm^{-2}]
Statistical	9.1×10^{15}	7.5×10^{15}	10.1×10^{15}	11.2×10^{15}
DOAS	7.8×10^{15}	8.0×10^{15}	9.2×10^{15}	12.2×10^{15}
SCD uncertainty (crf < 0.5)				
Statistical	9.3×10^{15}	7.8×10^{15}	10.2×10^{15}	11.9×10^{15}
DOAS	8.2×10^{15}	8.5×10^{15}	9.6×10^{15}	13.0×10^{15}

4.2 OMI NO_2 SCD uncertainty dependencies

The variability of the SCD uncertainty with latitude and the differences between the all-sky and clear-sky SCD uncertainty estimates prompt the investigation of dependencies of SCD uncertainty on potential drivers. The SCD uncertainty appears low for high latitudes, which could be caused by higher cloud fractions, SCDs, AMFs, reflectance levels, or a combination thereof at those latitudes. We binned the NO_2 statistical SCD uncertainties as a function of cloud fraction, SCD, AMF, and top-of-atmosphere reflectance (at 435 nm) for OMNO2A v1, v2, OMINO2-QA4ECV and OMNO2-NASA. Figure 7 shows that NO_2 SCD uncertainties from all algorithms decrease systematically with increasing cloud fraction, and, especially, with top-of-atmosphere reflectance, less with SCD, and not at all with AMF. The decrease of SCD uncertainty with cloud fraction is consistent with the lower SCD uncertainties for all-sky scenes listed in Table 4. The overall SCD uncertainties range from 0.5×10^{15} to 1.0×10^{15} molec. cm^{-2}., i.e. by a factor of 2. This suggests a more precise SCD determination when clouds are present. This holds for NO_2 DOAS SCD uncertainties for OMNO2A v1, v2 and QA4ECV (see Figure S2 in Supplement). NASA NO_2 DOAS uncertainties appear invariable with cloud fraction and top-of-atmosphere reflectance, but increase with SCD.

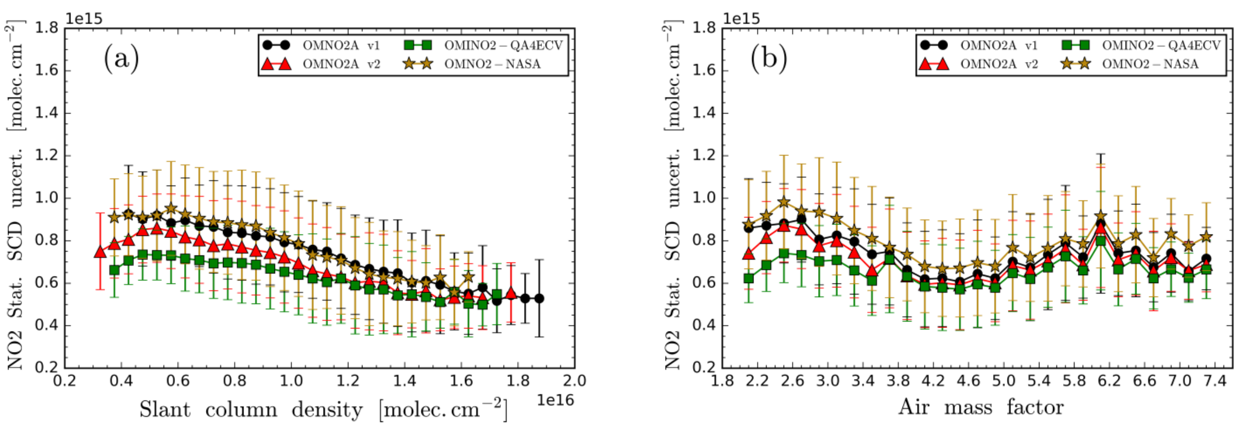

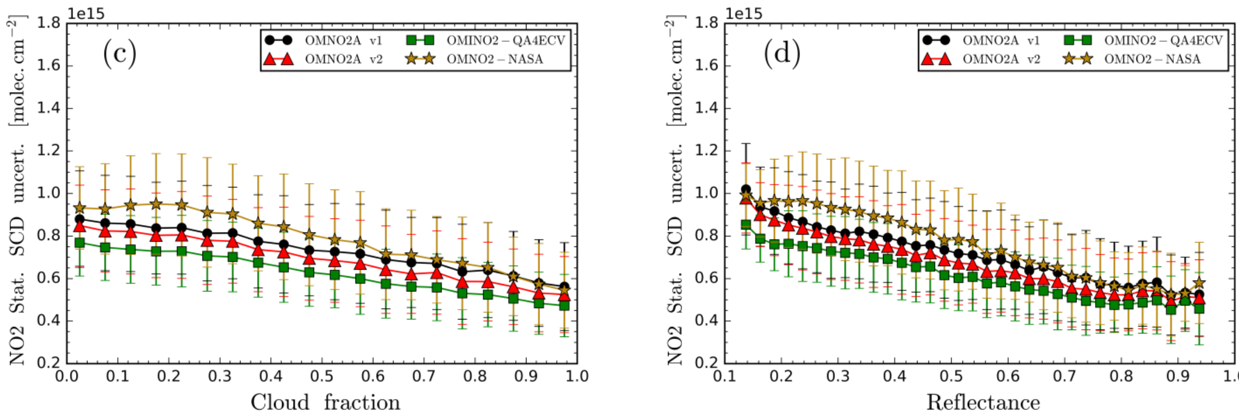

Figure 7. The statistical OMI NO_2 SCD uncertainty as a function of the (a) SCD, (b) AMF, (c) cloud fraction, and (d) the top-of-atmosphere reflectance for the OMNO2A v1 (black circles), OMNO2A v2 (red triangles), OMINO2-QA4ECV (green squares) and the OMNO2-NASA (yellow stars) SCDs for the Pacific orbit from day 01 of January, April, July and October (or closest available data) 2005-2015. Each bin contains at least 10 boxes for robust statistics and intercomparisons. Error bars represent one standard deviation (1σ).

The statistical NO_2 SCD uncertainties generally decrease with increasing SCD (Figure 7a). To investigate whether this is driven by the SCD itself ("more signal") or by the top-of-atmosphere reflectance levels ("better signal-to-noise"), we use a 3-step disentanglement scheme (~~Section S1~~ Figure S1 and Table S1 in ~~the~~ Supplement), which allows us to analyse whether SCD uncertainties for low and high reflectance scenes are significantly different when AMFs and SCDs are very similar. We find that for both OMINO2-QA4ECV and OMNO2-NASA the NO_2 SCD uncertainties are substantially higher for low-reflectance than for high-reflectance scenes. Over bright scenes, the OMINO2-QA4ECV SCD uncertainty is 35% lower than over dark scenes. This suggests that the top-of-atmosphere reflectance level is driving SCD uncertainties. We repeated the procedure to investigate whether SCD uncertainties for low and high SCD values are significantly different for pixels with very similar AMFs and top-of-atmosphere reflectance levels. We find that for OMINO2-QA4ECV the NO_2 SCD uncertainties for both low- and high- SCD values have similar values, suggesting that the SCD uncertainty does not depend on the SCD value. The OMNO2A v2 algorithm (not shown) yields similar results to OMINO2-QA4ECV for both schemes. This supports the hypothesis that signal-to-noise (high for high reflectances) rather than signal (SCD) strength is driving SCD uncertainties.

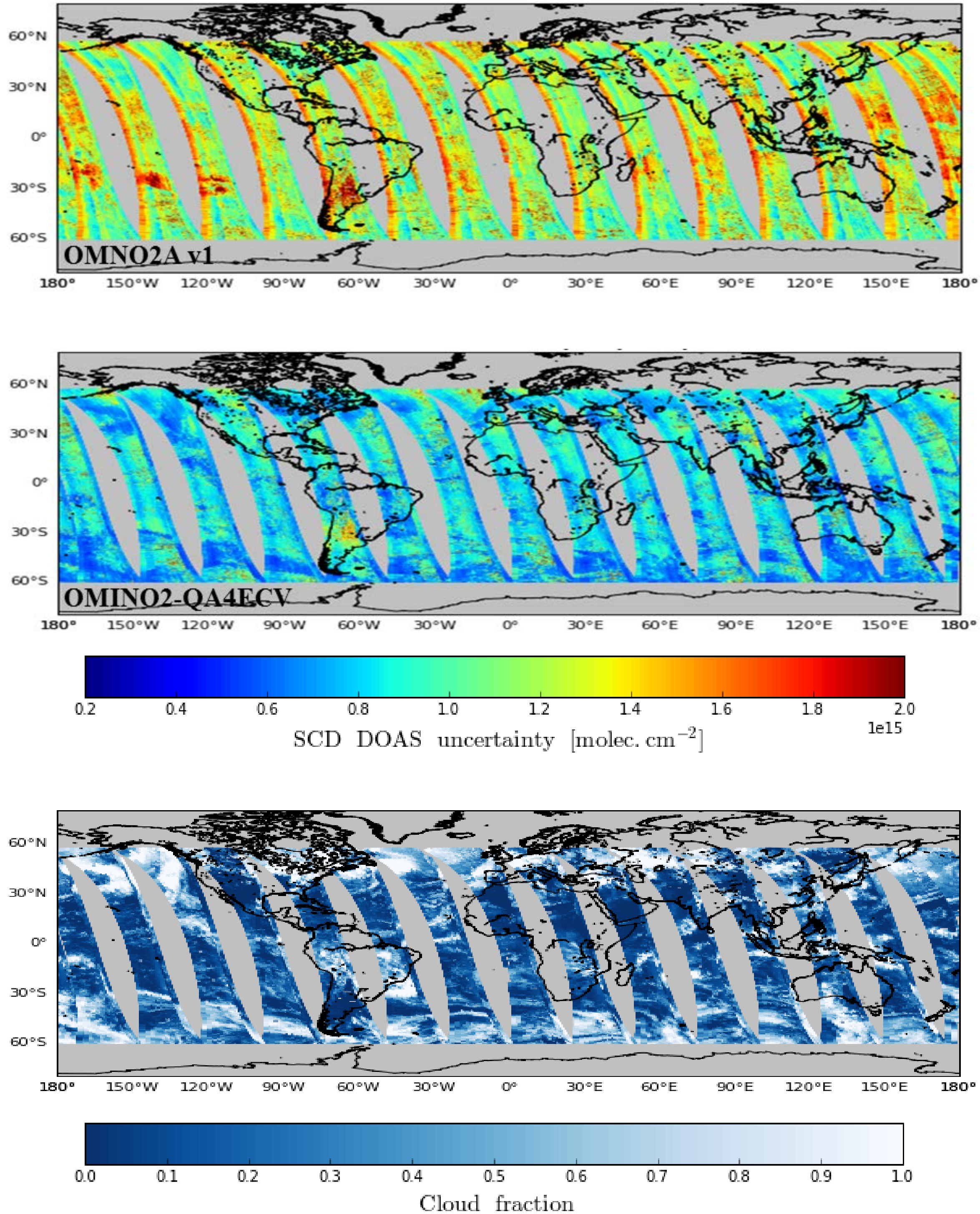

Figure 8. NO_2 DOAS SCD uncertainty from the OMNO2A v1 (top panel) and OMINO2-QA4ECV (middle panel) algorithms on 1 January, 2012. The bottom panel shows the cloud fractions from the OMCLDO2 retrieval for the same day.

This is also evident in Figure 8 where regions with high cloud fractions (such as 50°S-60°S) show low NO_2 (DOAS) SCD uncertainties. The OMINO2-QA4ECV SCD uncertainty (middle panel) is lower over scenes with higher cloud fraction (bottom panel)~~.~~ (or with higher top-of-atmosphere reflectance; see Figure S3 in Supplement). The bright(er) cloud surface enhances the intensity of the photons reaching the sensor (higher signal-to-noise), reducing the uncertainty in the SCD retrieval.

We see a general and significant improvement of the OMINO2-QA4ECV DOAS SCD uncertainties relative to OMNO2A v1 (top panel) on a global scale. Extreme SCD uncertainties at the edges of the swath are prominent in OMNO2A v1 but much reduced in OMINO2-QA4ECV. In OMNO2A v1 a fixed slit function for all 60 rows is used, whereas OMINO2-QA4ECV assigns a slit function for each across-track position individually. This improves spectral fitting for OMINO2-QA4ECV even for scenes under high viewing or solar zenith angles and bodes well for the use of the improved OMINO2-QA4ECV SCDs in the new OMI QA4ECV NO_2 ECV data product (www.qa4ecv.eu/ecvs).

4.3 Temporal evolution of SCD uncertainties

4.3.1 Trends in OMI NO_2 SCD uncertainties

In 2017 OMI has exceeded its anticipated lifespan by 7 years. Throughout the mission, the row anomaly, stripes and the instrument's radiometric degradation all affected the SCDs and their uncertainties. In this section we discuss possible changes in stability and quality of the DOAS fits throughout the 2005-2015 period. The optical degradation in the OMI visible channel is well below 5% over the mission so far (e.g. Boersma et al., 2011; QA4ECV Deliverable 4.2~~, 2016~~ [Müller et al., 2016], Schenkeveld et al., 2017). There are, however, clear signs of gradually increasing noise in the OMI radiances and irradiances mostly related to the long-term CCD performance (Schenkeveld et al., 2017), so we should anticipate a decrease in fitting quality over time. Figure 9 shows the evolution of the statistical and DOAS NO_2 SCD uncertainties for the OMNO2A v1, OMNO2A v2, OMINO2-QA4ECV and OMNO2-NASA algorithms. For all retrievals, SCD uncertainties show a weak positive trend (also see Table 7). The statistical SCD uncertainties for OMINO2-QA4ECV increase by 0.9%/yr relative to start, well below the ~2%/yr increase for the OMNO2A and OMNO2-NASA algorithms. The OMNO2-NASA DOAS uncertainties are virtually without trend (-0.3%/yr) in contrast with the statistical estimates. For clear-sky scenes, the rate of increase in the DOAS and statistical SCD uncertainties is somewhat higher relative to all-sky scenes for OMNO2A v1, v2 and OMINO2-QA4ECV (Table 7).

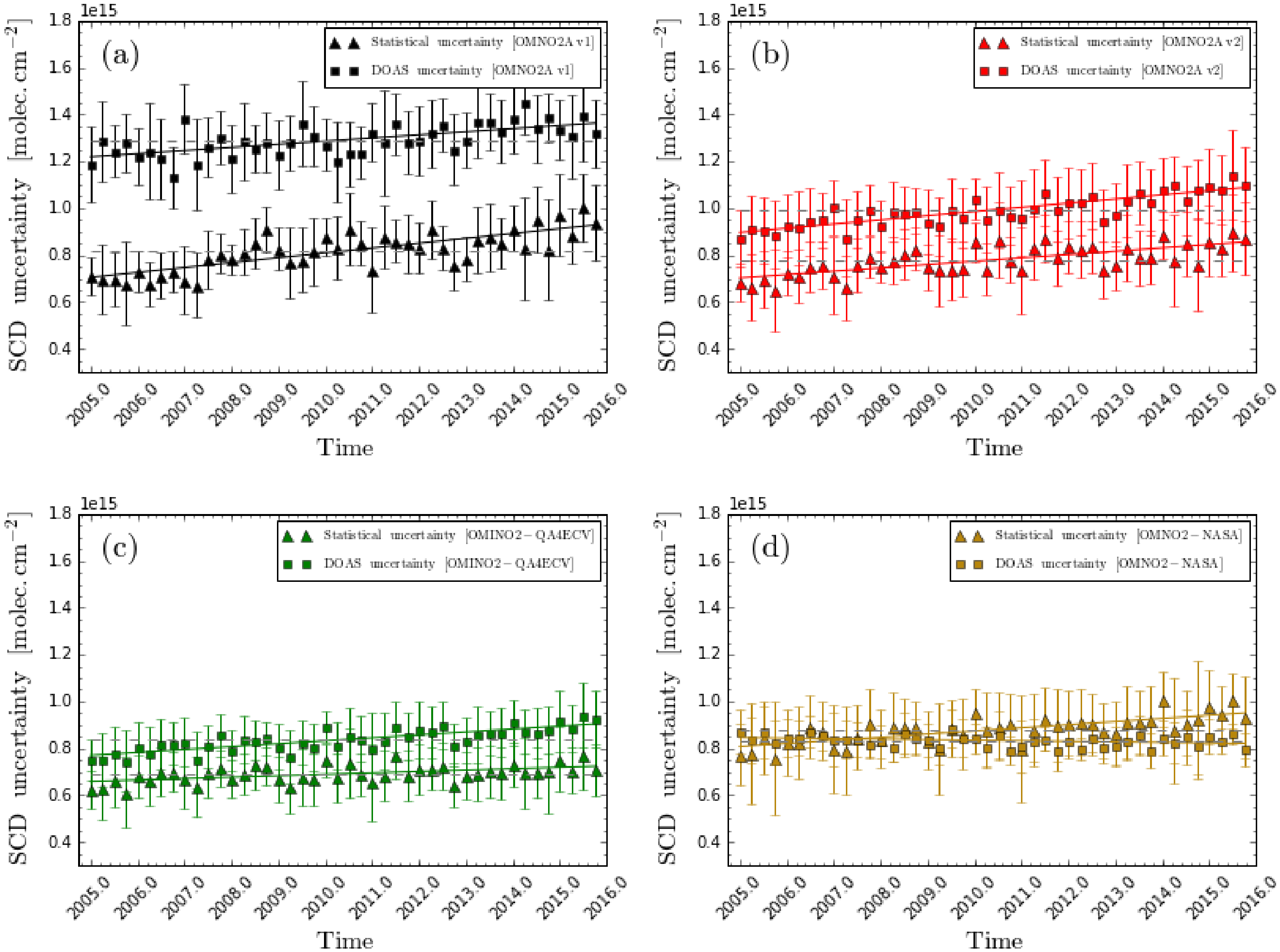

Figure 9. Temporal evolution of the statistical (triangles) and DOAS (squares) OMI NO_2 SCD uncertainty over 2005-2015 (Pacific orbit from day 1 of January, April, August, October) for OMNO2A v1 (black), OMNO2A v2 (red), OMINO2-QA4ECV (green) and OMNO2-NASA (yellow) algorithms. The solid line is the linear regression fitted to the data. The error bars represent one standard deviation (1σ). The slope, p, of each fit on the statistical, p^s, and DOAS uncertainty, p^d, is:

$p^{\mathrm{s}}_{\mathrm{v1}} = 0.021 \times 10^{15} \pm 0.003 \times 10^{15}$ molec. cm^{-2} yr^{-1} and $p^{\mathrm{d}}_{\mathrm{v1}} = 0.013 \times 10^{15} \pm 0.003 \times 10^{15}$ molec. cm^{-2} yr^{-1},

$p^{\mathrm{s}}_{\mathrm{v2}} = 0.014 \times 10^{15} \pm 0.002 \times 10^{15}$ molec. cm^{-2} yr^{-1} and $p^{\mathrm{d}}_{\mathrm{v2}} = 0.018 \times 10^{15} \pm 0.002 \times 10^{15}$ molec. cm^{-2} yr^{-1},

$p^{\mathrm{s}}_{\mathrm{qa4ecv}} = 0.006 \times 10^{15} \pm 0.002 \times 10^{15}$ molec. cm^{-2} yr^{-1} and $p^{\mathrm{d}}_{\mathrm{qa4ecv}} = 0.013 \times 10^{15} \pm 0.001 \times 10^{15}$ molec. cm^{-2} yr^{-1},

$p^{\mathrm{s}}_{\mathrm{nasa}} = 0.013 \times 10^{15} \pm 0.002 \times 10^{15}$ molec. cm^{-2} yr^{-1} and $p^{\mathrm{d}}_{\mathrm{nasa}} = 0.002 \times 10^{15} \pm 0.001 \times 10^{15}$ molec. cm^{-2} yr^{-1}.

Table 7. Yearly increase of the statistical and DOAS uncertainty estimates of OMI NO_2 SCDs for OMNO2A v1, v2, OMINO2-QA4ECV and OMNO2-NASA algorithms for the Pacific orbit from day 1 of January, April, July and October (or closest available data) 2005-2015 for all-sky conditions (top panel) and clear-sky conditions (bottom panel).

SCD uncertainty (all-sky)	OMNO2A v1 [yr^{-1}]	OMNO2A v2 [yr^{-1}]	OMINO2-QA4ECV [yr^{-1}]	OMNO2-NASA [yr^{-1}]
Statistical	2.9%	2.0%	0.9%	1.7%
DOAS	1.1%	2.0%	1.6%	-0.3%
SCD uncertainty (crf < 0.5)				
Statistical	3.2%	2.3%	1.0%	1.3%
DOAS	1.3%	2.2%	1.9%	-0.1%

OMI shows low optical degradation and high wavelength stability over the mission lifetime. One can thus raise the question why the SCD uncertainty increases in time since OMI, apart from the RA, continues to perform well (Schenkeveld et al., 2017). Increases in dark-current are monitored and corrected for daily, so these are unlikely to contribute to the trend. Increases in the random telegraph signal cannot be corrected for (N. Rozemeijer, priv. comm., 2017), and may contribute to a trend in SCD uncertainties. The number of pixels flagged as “bad” (those with off-nominal behaviour) has increased to 11%. Furthermore, stripes are apparent in trace gas column retrievals since the beginning of the mission, and their magnitude has increased over time (Boersma et al., 2011).

In Section 4.1.3 we saw that the NO_2 DOAS SCD uncertainty generally exceeds the statistical uncertainty reflecting persistent systematic uncertainty in the DOAS fit. We investigate here the amount of uncertainty in the total NO_2 SCD uncertainty originating from stripes. This stripe-induced uncertainty is estimated as the root-mean-square of the stripe correction for rows 0-21 and 54-59 per OMINO2-QA4ECV orbit. Figure 10 (left panel) shows the stripe-induced uncertainty increase from 0.33×10^{15} to 0.48×10^{15} molec. cm^{-2} over 2005-2015 (a 45% increase). Hence, we subtract[6] (Figure 10; right panel) the contribution from stripes from the total NO_2 SCD (DOAS) uncertainty.

[6]The stripe-induced uncertainty, ε_{str}, is subtracted from the total SCD uncertainty (i.e. DOAS uncertainty), ε_{tot}, by the prescription: $\sqrt{\varepsilon_{tot}^2 - \varepsilon_{str}^2} = \varepsilon_{w/o}$, where $\varepsilon_{w/o}$ is the SCD (DOAS) uncertainty without the contribution from stripes.

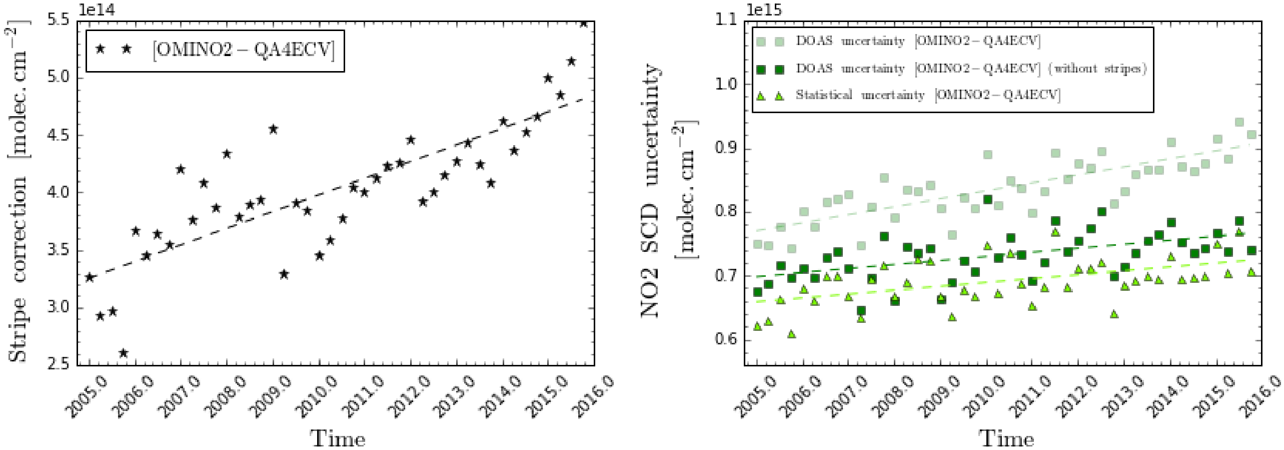

Figure 10. (left) Temporal evolution of the stripe-induced SCD uncertainty for OMINO2-QA4ECV. (right) Temporal evolution of the NO_2 DOAS SCD uncertainty for OMINO2-QA4ECV before (light green squares; as seen in Figure 9c)) and after (dark green squares) the subtraction of the stripe-induced SCD uncertainty. The green triangles represent the temporal evolution of the NO_2 statistical SCD uncertainty (as seen in Figure 9c).

Total NO_2 SCD (DOAS) uncertainties for OMINO2-QA4ECV increases by 17.5% over 11 years. After subtracting the contribution from stripes, the SCD uncertainties increase by 9.8% over the same time period, closer to what is expected from the radiometric degradation. Accounting for stripes reduces the systematic component to the total uncertainty by ~70%, and the DOAS and statistical uncertainty estimates are now in better agreement (within 6%, Figure 10; right). The statistical and DOAS uncertainty now follow the same increase rate (0.9%/yr), suggesting that stripes explain much of the discrepancy between the DOAS and statistical uncertainty estimates (Figure 3(c)). The origin of the stripes is not well known but it is most likely associated with noise and instrument-related artefacts in the solar irradiance spectrum. ~~This~~ The presence of stripes manifests when a fixed solar spectrum (2005 annual mean for OMNO2A and OMINO2-QA4ECV) is used as reference for all years, so that the representativeness of that spectrum is reduced in years later than 2005. This is supported by the use of a daily Earth radiance spectrum as reference rather than a fixed irradiance spectrum in OMIHCHO-QA4ECV resulting in much weaker increases in OMI HCHO SCD uncertainty (0.3%/yr). Anand et al. [2015] also pointed out this (and other) benefits from using an Earth radiance reference rather than solar irradiance spectra. For future NO_2 spectral fitting algorithms the choice of radiance over irradiance spectra as reference is debatable; on the one hand the SCDs will suffer significantly less from stripes, but on the other the retrieved SCDs will no longer be 'absolute' SCDs rather than 'differential'. A background correction would be required to convert differential SCDs to absolute SCDs by adding an observed climatological or modelled stratospheric slant column. As a compromise, the NASA retrieval uses monthly-averaged solar data (Marchenko et al., 2015).

4.3.2 Trends in GOME-2A NO_2 SCD uncertainties

We now investigate the performance of the BIRA and QA4ECV DOAS fits for GOME-2A throughout 2007-2015. Both GONO2A-QA4ECV DOAS and statistical uncertainties are lower than BIRA, but they still show a substantial positive trend (Figure 11). Starting from values of ~0.4-0.6×10^{15} molec. cm^{-2} in 2007, the statistical and DOAS uncertainty increase by 57% and 45% (relative to start) by the end of 2015 for GONO2A-QA4ECV. This corresponds to an annual increase rate of ~7%/yr (statistical) and ~5%/yr (DOAS) for the uncertainty (Figure S4 and Table S2 in Supplement), notably higher than what was found for OMI (Table 7). A continuous spectrally dependent throughput degradation (UV: 20%/year; VIS: 10%/year) has been observed since GOME-2A launch in 2007. In September 2009, a 2nd throughput test was performed (1st test was in January 2009). The second test caused an additional throughput decrease of 25% in the UV and 10% in the visible. Despite the substantial throughput loss, the test also stabilized GOME-2A degradation. The reported linear degradation rate after the second throughput test in September 2009 fell to ~3%/year for the UV-channel and 1% for the visible. Munro et al. [2016] and Beirle et al. [2017] also reported a general long-term drift of the instrument's ~~spectral response~~ slit function~~ (ISRF)~~, a key quantity for wavelength calibration and for convolution of the cross sections to the sensor's resolution. These ~~ISRF~~ changes are ~~strongly~~ considerably weakened after the test and the ~~ISRF~~ slit function appears quite stable. Motivated by GOME-2A continuous degradation and the 2nd throughput test in September 2009 with the positive effects reported on the quality of the level-1 data (EUMETSAT: Investigation on GOME-2 Throughput Degradation, 2011)~~ on the quality of the level-1 data~~, we performed linear regressions for two sub-periods; before and after the 2nd throughput test. The reduction in fitting quality for GONO2A-BIRA and GONO2A-QA4ECV appears to proceed at a much higher pace before the 2nd throughput test (9-12%/yr) than after (2-4%/yr) (Table 8), consistent with the reported degradation rate for the visible channel before (1~~0~~1%/yr) and after (1%/yr) the test. The reduction of the uncertainty increase rate is even stronger for clear-sky scenes. GOME-2A HCHO SCD uncertainties show similar behaviour; before the test the uncertainty increases at a pace of 12-17%/yr (20%/yr reported for the UV) while after the test the increase rate is 1-4%/yr (3%/yr reported for the UV).

On 15 July 2013, GOME-2A pixel sizes were reduced from 80×40 km^2 to 40×40 km^2. With the integration time for each detector pixel remaining the same, the SCD uncertainties between July 2013 and December 2015 have not changed relative to the period September 2009-July 2013. Table 8 summarizes the trends in GOME-2A NO_2 SCD uncertainties.

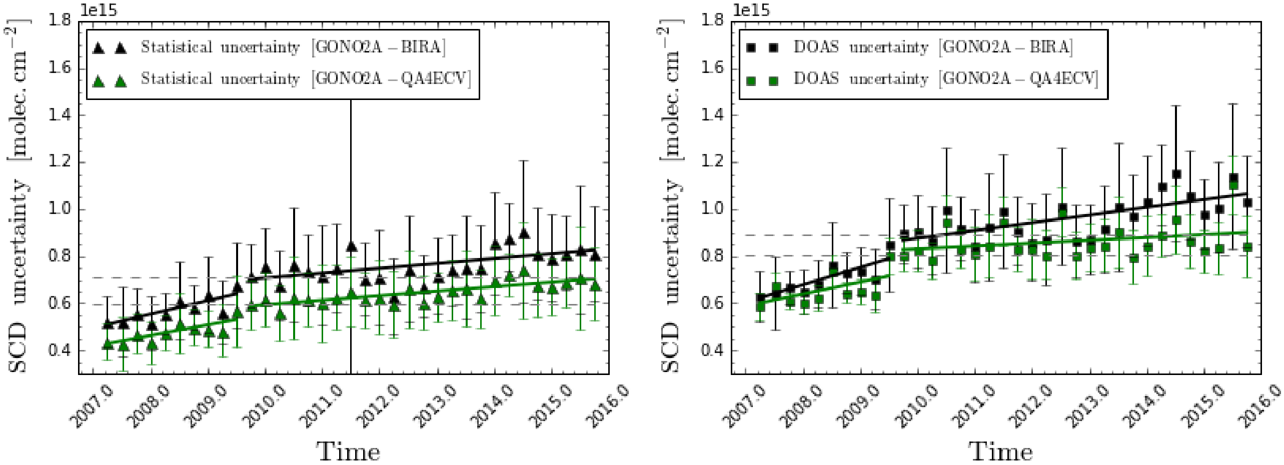

Figure 11. Temporal evolution of the statistical (triangles) and DOAS (squares) GOME-2A NO_2 SCD uncertainty for the sub-periods before and after the 2[nd] throughput test (September 2009) for GONO2A-BIRA (black) and GONO2A-QA4ECV (green) (Pacific orbit from day 1 of January, April, August, October- or closest available data 2007-2015). Error bars represent one standard deviation (1σ). Solid lines represent the linear fitted regressions fitted to the data for each sub-period (Table 8). The slope, p, of each fit on the statistical, p^s, and DOAS uncertainty, p^d, is:

Before the test:

$$p^{\mathrm{s}}_{\mathrm{bira}} = 0.057 \times 10^{15} \pm 0.017 \times 10^{15}\ \mathrm{molec.\,cm^{-2}\ yr^{-1}} \text{ and } p^{\mathrm{d}}_{\mathrm{bira}} = 0.074 \times 10^{15} \pm 0.019 \times 10^{15}\ \mathrm{molec.\,cm^{-2}\ yr^{-1}},$$

$$p^{\mathrm{s}}_{\mathrm{qa4ecv}} = 0.046 \times 10^{15} \pm 0.013 \times 10^{15}\ \mathrm{molec.\,cm^{-2}\ yr^{-1}} \text{ and } p^{\mathrm{d}}_{\mathrm{qa4ecv}} = 0.051 \times 10^{15} \pm 0.029 \times 10^{15}\ \mathrm{molec.\,cm^{-2}\ yr^{-1}}.$$

After the test:

$$p^{\mathrm{s}}_{\mathrm{bira}} = 0.021 \times 10^{15} \pm 0.007 \times 10^{15}\ \mathrm{molec.\,cm^{-2}\ yr^{-1}} \text{ and } p^{\mathrm{d}}_{\mathrm{bira}} = 0.033 \times 10^{15} \pm 0.008 \times 10^{15}\ \mathrm{molec.\,cm^{-2}\ yr^{-1}},$$

$$p^{\mathrm{s}}_{\mathrm{qa4ecv}} = 0.019 \times 10^{15} \pm 0.003 \times 10^{15}\ \mathrm{molec.\,cm^{-2}\ yr^{-1}} \text{ and } p^{\mathrm{d}}_{\mathrm{qa4ecv}} = 0.012 \times 10^{15} \pm 0.008 \times 10^{15}\ \mathrm{molec.\,cm^{-2}\ yr^{-1}}.$$

Table 8. Yearly increase of the statistical and DOAS uncertainty estimates for the sub-periods before and after the 2[nd] throughput test (September 2009) for GOME-2A NO_2 SCDs from GONO2A-BIRA and GONO2A-QA4ECV (Pacific orbit from day 1 of January, April, August, October- or closest available data 2007-2015) for all-sky conditions (top panel) and clear-sky conditions (bottom panel).

SCD uncertainty (all-sky)	GONO2A-BIRA (before) [yr^{-1}]	GONO2A-QA4ECV (before) [yr^{-1}]	GONO2A-BIRA (after) [yr^{-1}]	GONO2A-QA4ECV (after) [yr^{-1}]
Statistical	11.2%	10.7%	2.9%	3.3%
DOAS	11.9%	8.5%	3.8%	1.5%
SCD uncertainty (crf < 0.5)				
Statistical	12.4%	14.2%	3.3%	2.6%
DOAS	14.0%	11.9%	3.7%	1.7%

4.3.3 Trends in OMI and GOME-2A HCHO SCD uncertainties

Figure 12 shows the evolution of the statistical uncertainty for OMIHCHO and GO2AHCHO. For OMI, the statistical uncertainty estimates show a weak positive trend of 0.5%/yr and 0.4%/yr for OMIHCHO-QA4ECV and OMIHCHO-BIRA relative to start, respectively. This confirms the remarkable stability of the OMI level-1 data, and suggests that these OMI HCHO retrievals are in principle useful for the detection of trends in HCHO columns. Potential impact of spectral interferences of O_3 and BrO absorption features on the HCHO fit (e.g. González et al., 2015), and conceivably on the HCHO trends, is largely mitigated by the background correction scheme. Due to the nature of this correction, only geographically localized O_3 and BrO trends coincidental with high HCHO emission regions could affect the corrected HCHO columns. Such effects, if any, are unlikely to lead to pervasive, substantial biases in HCHO trend analyses.

The situation is quite different for GOME-2A. Overall, the statistical QA4ECV HCHO SCD uncertainties increased from ~8×10^{15} to 14×10^{15} molec. cm^{-2} (2007-2015), which corresponds to ~8%/yr relative to start (Figure S5 and Table S3 in Supplement). The effect of the throughput test in September 2009 is evident: after the test, the QA4ECV SCD uncertainties increased only by 1-2%/yr, a clear improvement from the 12-17%/yr degradation (2× the rate observed in GOME-2A NO_2) before the test (Figure 12 and Table 9).

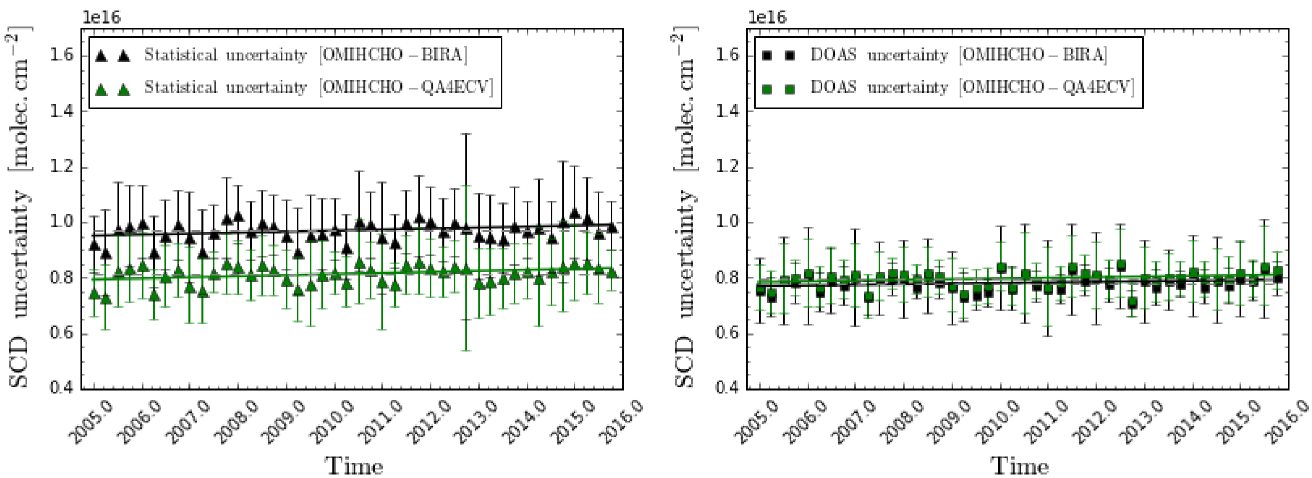

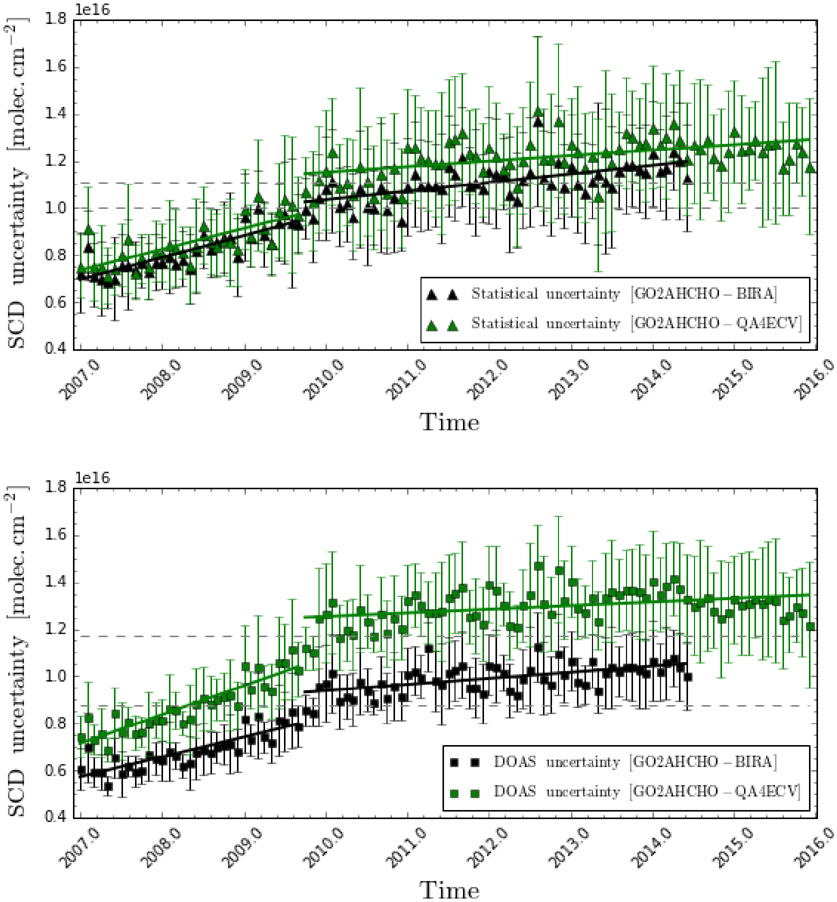

Figure 12. Temporal evolution of the statistical (triangles) and DOAS (squares) OMI and GOME-2A HCHO SCD uncertainty for OMIHCHO-BIRA (black) and OMIHCHO-QA4ECV (green) (Pacific orbit from day 1 of January, April, July and October (or closest available data) 2005-2015), and GO2AHCHO-BIRA (black) and GO2AHCHO-QA4ECV (green) (Pacific orbit from day 1 of January up to December and from day 15 of January, April, July and October 2007-June 2014 and 2007-2015, respectively) for the sub-periods before and after the 2nd throughput test (September 2009). Error bars represent one standard deviation (1σ). Solid lines represent the linear fitted regressions fitted to the data for each sub-period (Table 8). The slope, p, of each fit on the statistical, p^s, and DOAS uncertainty, p^d, for OMIHCHO is:

$p^{\mathrm{s}}_{\mathrm{bira}} = 0.04 \times 10^{15} \pm 0.02 \times 10^{15}$ molec. cm^{-2} yr^{-1} and $p^{\mathrm{d}}_{\mathrm{bira}} = 0.02 \times 10^{15} \pm 0.01 \times 10^{15}$ molec. cm^{-2} yr^{-1},

$p^{\mathrm{s}}_{\mathrm{qa4ecv}} = 0.04 \times 10^{15} \pm 0.02 \times 10^{15}$ molec. cm^{-2} yr^{-1} and $p^{\mathrm{d}}_{\mathrm{qa4ecv}} = 0.02 \times 10^{15} \pm 0.01 \times 10^{15}$ molec. cm^{-2} yr^{-1} ,

and for GO2AHCHO before the test is:

$p^{\mathrm{s}}_{\mathrm{bira}} = 0.92 \times 10^{15} \pm 0.11 \times 10^{15}$ molec. cm^{-2} yr^{-1} and $p^{\mathrm{d}}_{\mathrm{bira}} = 0.84 \times 10^{15} \pm 0.10 \times 10^{15}$ molec. cm^{-2} yr^{-1},

$p^{\mathrm{s}}_{\mathrm{qa4ecv}} = 0.88 \times 10^{15} \pm 0.14 \times 10^{15}$ molec. cm^{-2} yr^{-1} and $p^{\mathrm{d}}_{\mathrm{qa4ecv}} = 1.22 \times 10^{15} \pm 0.11 \times 10^{15}$ molec. cm^{-2} yr^{-1},

and after the test is:

$p^{\mathrm{s}}_{\mathrm{bira}} = 0.03 \times 10^{15} \pm 0.06 \times 10^{15}$ molec. cm^{-2} yr^{-1} and $p^{\mathrm{d}}_{\mathrm{bira}} = 0.26 \times 10^{15} \pm 0.05 \times 10^{15}$ molec. cm^{-2} yr^{-1},

$p^{\mathrm{s}}_{\mathrm{qa4ecv}} = 0.23 \times 10^{15} \pm 0.05 \times 10^{15}\ \mathrm{molec.\,cm^{-2}\,yr^{-1}}$ and $p^{\mathrm{d}}_{\mathrm{qa4ecv}} = 0.15 \times 10^{15} \pm 0.04 \times 10^{15}\ \mathrm{molec.\,cm^{-2}\,yr^{-1}}$.

Figure 12 suggests that the GO2AHCHO-QA4ECV deteriorates more than GO2AHCHO-BIRA, especially after the 2nd throughput test. This is mainly due to the fact that GO2AHCHO-QA4ECV uses a larger fitting window, and that GOME-2A radiances contain polarization structures in this interval. To reduce polarization- related systematic errors, pseudo cross-sections have been included in the fit, which results in somewhat increased random uncertainty (and systematic uncertainty if not perfectly mitigated by the background correction) in the HCHO SCDs. Despite the increase in the random uncertainty, the SCD uncertainty increases at a slower pace suggesting the GOME-2A HCHO retrievals will allow the detection of trends in HCHO columns, challenging nevertheless.

Table 9. Yearly increase of the statistical and DOAS uncertainty estimates of OMI and GOME-2A HCHO SCDs for OMIHCHO-BIRA and OMIHCHO-QA4ECV (Pacific orbit from day 1 of January, April, August, October- or closest available data 2007-2015), and GONO2A-BIRA and GONO2A-QA4ECV (Pacific orbit from day 1 of January up to December and from day 15 of January, April, July and October 2007-June 2014 and 2007-2015, respectively) for the sub-periods before and after the 2nd throughput test (September 2009), for all-sky conditions (top panel) and clear-sky conditions (bottom panel). The GO2AHCHO-BIRA data are provided only for scenes with cloud fraction lower than 0.4, therefore the clear-sky conditions yield similar SCD uncertainties to the all-sky conditions.

SCD uncertainty (all-sky)	OMIHCHO-BIRA [yr^{-1}]	OMIHCHO-QA4ECV [yr^{-1}]	GO2AHCHO-BIRA (before) [yr^{-1}]	GO2AHCHO-QA4ECV (before) [yr^{-1}]	GO2AHCHO-BIRA (after) [yr^{-1}]	GO2AHCHO-QA4ECV (after) [yr^{-1}]
Statistical	0.4%	0.5%	13.3%	12.0%	3.5%	2.0%
DOAS	0.3%	0.3%	14.7%	17.1%	2.8%	1.2%
SCD uncertainty (crf < 0.5)						
Statistical	0.4%	0.5%	13.5%	13.3%	3.8%	3.7%
DOAS	0.5%	0.5%	14.6%	16.9%	2.8%	2.7%

4.3.4 Implication for stability of long-term tropospheric NO_2 ECV datasets

According to GCOS, the user requirement for stability is a requirement on the extent to which the uncertainty of a measurement remains constant over a long period (GCOS-200, 2016). GCOS-200 defines ‘uncertainty (of measurement)’ as the parameter that characterizes the dispersion of the values that could reasonably be attributed to the measured quantity. The relevant component of the uncertainty of a measurement for climate application is often the systematic error and its maximum acceptable change, usually per decade, and it is defined by the mean error over a period such as a month or year. GCOS-154 defines 'error' as the difference between measurement value and true value. We cannot assess the stability of the main (tropospheric column) product here, as this would require a major validation effort to assess a possible drift of the tropospheric column bias in time. We may however investigate the increases of SCD uncertainties in time, and evaluate to what extent changes in noise would still allow meaningful trend analysis in tropospheric and stratospheric columns.

Stratospheric NO_2 columns

The recent retrieval developments (e.g. the systematic reduction in SCDs by ~~±~~~1.2×10^{15} molec. cm^{-2} along with a 30% reduction of fitting errors from OMNO2A v1 to v2 in Van Geffen et al. [2015]) and the QA4ECV-driven improvements reported here (Figures 1 and 3) suggest that at least part of the SCD uncertainty is systematic rather than random, but also that such systematic effects can be removed. If we consider the SCD uncertainties to be completely systematic~~ in nature~~, then we should regard the DOAS SCD uncertainties as a lower limit for trends in stratospheric NO_2 that can be reliably detected from stratospheric NO_2 column time series. This would imply that from e.g. the QA4ECV OMI dataset, one can infer only trends in stratospheric NO_2 columns larger than 0.3-0.4$\times10^{15}$ molec.~~ules~~ cm^{-2}/decade (SCD uncertainty divided by typical stratospheric AMF). In practice, however, the DOAS SCD uncertainty as we know it consists of a random (from level-1 noise) and systematic (primarily from stripes) part, as shown in Section 4.3.1. The random component of the SCD uncertainty can be reduced to virtually zero by averaging over space and time. The differences between the total DOAS SCD uncertainty (with random + systematic contributions) and statistical SCD uncertainty (random component), as shown in Figures 3 and 10 ($\varepsilon^2 - \varepsilon_r^2 = \varepsilon_s^2$), then provide a lower limit of trend detection (from systematic uncertainty) in OMI stratospheric NO_2 columns down to 0.1-0.2$\times10^{15}$ molec.~~ules~~ cm^{-2}/decade.

Tropospheric NO_2 retrievals

Uncertainty in the SCD does not directly translate into tropospheric column uncertainty as it does for stratospheric column uncertainty. The tropospheric retrieval is based on the difference between the DOAS SCDs and estimated stratospheric SCDs, as well as various factors related to the AMF evaluation. Since the stratospheric SCDs depend on the DOAS SCDs (e.g. Dirksen et al., 2011; Beirle et al., 2016), additive systematic offsets in the SCDs will largely cancel in the tropospheric residual SCD. In Van Geffen et al. [2015], spectral fitting retrieval improvements were shown to be mostly additive, suggesting that systematic components of the SCD uncertainty are of less relevance for NO_2 tropospheric column retrievals. Marchenko et al. [2015] discussed the possibility of a considerable systematic, multiplicative factor (between OMNO2A v1 and OMNO2-NASA), and such a component, if real, would be relevant for NO_2 tropospheric column retrievals and their usefulness for trend detection. The instability in the SCDs because of stripes (OMI) or instrument degradation (GOME-2A) ~~could be~~was evaluated further by testing the robustness of the tropospheric signal over a well-chosen reference area with little known pollution. We find that for OMI and GOME-2A the monthly mean tropospheric NO_2 columns are stable throughout 2005(7)-2015 with no significant trend over a pristine region (see Figure S6 in Supplement).

In the absence of a substantial systematic, multiplicative error in the NO_2 SCDs, the stability of tropospheric NO_2 vertical columns will therefore be dominated by instability in AMF uncertainties. For instance, if assumptions on surface albedo or a priori NO_2 profile shape grow increasingly inaccurate over time (because of e.g. urbanization, increasing aerosol haze, change in vegetation), this will lead to growing systematic uncertainties in tropospheric AMFs (Lamsal et al., 2015). Such systematic, or structural, uncertainties may increase to up to 30-40% in rapidly changing regions such as parts of India and China (Lorente et al., 2017).

5 Conclusions

Recently improved spectral fitting algorithms for OMI and GOME-2A developed by BIRA-IASB, IUP and KNMI as part of the QA4ECV consortium and also by NASA for OMI have generated new datasets of NO_2 and HCHO slant columns that are the starting point for improved retrievals of tropospheric columns, and whose quality determines the effective detection limit and usefulness for trend detection and emission estimates from the retrievals. These new datasets have not yet been quality assured, which is important in view of the known degradation of the instruments. We compared NO_2 and HCHO slant columns retrieved from the OMI and GOME-2A instruments throughout much of their operational periods (2005-2015), and paid special attention to the characterization of their uncertainties.

The new QA4ECV NO_2 and HCHO spectral fitting algorithm is an improvement over previous approaches by performing a wavelength calibration to the full fitting window width, and by extending the fitting equation with an intensity offset term that accounts for possible effects from stray-light, instrumental thermal instabilities, or dark current changes. We find that the new QA4ECV NO_2 slant columns agree very well (within 2%) with slant column data from KNMI (OMNO2A v2) and BIRA (QDOAS) for both OMI and GOME-2A. New OMI NASA NO_2 slant columns (v3.1) are also in good agreement with those from QA4ECV and KNMI. For HCHO, we find very good consistency between the QA4ECV and BIRA (differential) datasets.

The improved quality of the QA4ECV OMI and GOME-2A NO_2 slant columns is underlined by their low statistical uncertainties; $0.7\text{-}0.8\times10^{15}$ molec. cm^{-2} for OMI and for GOME-2A on average for clear-sky scenes. These uncertainties are lower than those from the OMNO2A v2, NASA, and BIRA algorithms ($\sim0.9\times10^{15}$ molec. cm^{-2}). HCHO slant column uncertainties are also lower for OMI QA4ECV (8×10^{15} down from 9×10^{15} molec. cm^{-2}), but not for GOME-2A, related to the use of a larger fitting window requiring the use of ad-hoc corrections for spectral polarization structures. We used a statistical approach that quantifies the variability of the slant columns over pristine areas as an independent test of the DOAS uncertainties. For HCHO, we find excellent agreement between the statistical and the DOAS uncertainty estimates, suggesting that the fitting uncertainty is dominated by random noise in the satellite level-1 data for that species. This is not so for NO_2, where the DOAS uncertainty estimates are systematically higher than the statistical ones, suggesting that the DOAS uncertainties for NO_2 include both a random (~65% of the total uncertainty) and a systematic part (~3~~0~~5% of the total uncertainty). We found that stripes, increasing over time, can largely explain the discrepancy between statistical and DOAS uncertainties for OMI. This discrepancy diminishes in the HCHO uncertainties because of the use of radiance instead of irradiance spectra as reference in the fit.

The slant column uncertainties are driven primarily by the magnitude of the top-of-atmosphere reflectance. For relatively dark scenes corresponding to mostly cloud-free scenes and low surface albedo, NO_2 uncertainties are up to 2× higher than those over bright scenes. This confirms the notion that sufficiently high signal-to-noise levels of level-1 (radiance) spectra are required for good quality fits. Our analysis of trends in the NO_2 and HCHO slant column uncertainties corroborates this: for the radiometrically stable OMI sensor, we find only minor increases in fitting uncertainty throughout the mission period (increases of 1-2%/yr for NO_2), but for GOME-2A the SCD uncertainties increase by 12-14%/yr (for clear-sky scenes) up until September 2009 when a test for throughput loss was performed. After this test, which initially resulted in an additional loss of signal-to-noise, GOME-2A NO_2 SCD uncertainties increase at a slower pace of 2-3%/yr.

The increasing slant column uncertainties are indicative of the stability of the stratospheric and tropospheric (NO_2) column retrievals. Because the slant column uncertainty is dominated by random contributions from the propagation of measurement noise, much of it can be reduced by averaging over space, or in time, and trend detection in stratospheric NO_2 down to the ~1%/decade level should be well possible with all four OMI fitting algorithms. The stability of the long-term tropospheric NO_2 record is likely limited by instability in AMF uncertainties rather than in the weak increases in SCD uncertainties reported here.

Our work points to the need for detailed validation of the new satellite data products from KNMI, NASA and QA4ECV. Dedicated validation efforts could point out whether any systematic biases in the tropospheric columns are sufficiently constant over longer periods, and could help in attributing any biases to their underlying causes in the retrieval chain. The QA4ECV NO_2 and HCHO data products have been released publicly and registered (Boersma et al. [2017[a]]; Boersma et al. [2017[b]]; De Smedt et al. [2017]), and the data sets can be found online (www.qa4ecv.eu/ecvs).

Acknowledgments

This research was funded by the FP7 EU Project Quality Assurance for Essential Climate Variables (QA4ECV), grant No. 607405.

References

Anand, J. S., Monks, P. S., and Leigh, R. J.: An improved retrieval of tropospheric NO2 from space over polluted regions using an Earth radiance reference, Atmos. Meas. Tech. ,8, 1519–1535, doi:10.5194/amt-8-1519-2015, 2015.

Bauer, S. E., Koch, D., Unger, N., Metzger, S. M., Shindell, D. T., and Streets, D. G.: Nitrate aerosols today and in 2030: a global simulation including aerosols and tropospheric ozone, Atmos. Chem. Phys., 7, 5043-5059, doi:10.5194/acp-7-5043-2007, 2007.

Beirle, S., Hörmann, C., Jöckel, P., Liu, S., Penning de Vries, M., Pozzer, A., Sihler, H., Valks, P. and Wagner, T.: The STRatospheric Estimation Algorithm from Mainz (STREAM): estimating stratospheric NO2 from nadir-viewing satellites by weighted convolution, Atmos. Meas. Tech., 9(7), 2753–2779, doi:10.5194/amt-9-2753-2016, 2016.

Beirle, S., Lampel, J., Lerot, C., Sihler, H., and Wagner, T.: Parameterizing the instrumental spectral response function and its changes by a super-Gaussian and its derivatives, Atmos. Meas. Tech., 10, 581–598, doi:10.5194/amt-10-581-2017, 2017.

Boersma, K. F., Eskes, H. J., and Brinksma, E. J.: Error analysis for tropospheric NO2 retrieval from space, J. Geophys. Res., 109, D04311, doi:10.1029/2003JD003962, 2004.

Boersma, K. F., Eskes, H. J., Veefkind, J. P., Brinksma, E. J., Van der A, R. J., Sneep, M., Van den Oord, G. H. J., Levelt, P. F., Stammes, P., Gleason, J. F., and Bucsela, E. J.: Near-real time retrieval of tropospheric NO2 from OMI, Atmos. Chem. Phys., 7, 2103–2118, doi:10.5194/acp-7-2103-2007, 2007.

Boersma, K. F., Eskes, H. J., Dirksen, R. J., Van der A, R. J., Veefkind, J. P., Stammes, P., Huijnen, V., Kleipool, Q. L., Sneep, M., Claas, J., Leitão, J., Richter, A., Zhou, Y., and Brunner, D.: An improved tropospheric NO2 column retrieval algorithm for the Ozone Monitoring Instrument, Atmos. Meas. Tech., 4, 1905–1928, doi:10.5194/amt-4-1905-2011, 2011.

Boersma, K. F., Eskes, H., Richter, A., De Smedt, I., Lorente, A., Beirle, S., Van Geffen, J., Peters, E., Van Roozendael, M. and Wagner, T.: QA4ECV NO_2 tropospheric and stratospheric vertical column data from OMI (Version 1.1) [Data set]. Royal Netherlands Meteorological Institute (KNMI), http://doi.org/10.21944/qa4ecv-no2-omi-v1.1, 2017[a].

Boersma, K. F., Eskes, H., Richter, A., De Smedt, I., Lorente, A., Beirle, S., Van Geffen, J., Peters, E., Van Roozendael, M. and Wagner, T.: QA4ECV NO_2 tropospheric and stratospheric vertical column data from GOME-2A (Version 1.1) [Data set]. Royal Netherlands Meteorological Institute (KNMI), http://doi.org/10.21944/qa4ecv-no2-gome2a-v1.1, 2017b.

Bucsela, E. J., Celarier, E., Wenig, M., Gleason, J., Veefkind, J., Boersma, K., and Brinksma, E.: Algorithm for NO2 vertical column retrieval from the ozone monitoring instrument, Geoscience and Remote Sensing, IEEE Trans., 44, 1245–1258, doi:10.1109/TGRS.2005.863715, 2006.

Bucsela, E. J., Krotkov, N. A., Celarier, E. A., Lamsal, L. N., Swartz, W. H., Bhartia, P. K., Boersma, K. F., Veefkind, J. P., Gleason, J. F., and Pickering, K. E.: A new stratospheric and tropospheric NO2 retrieval algorithm for nadir-viewing satellite instruments: applications to OMI, Atmos. Meas. Tech., 6, 2607–2626, doi:10.5194/amt-6-2607-2013, 2013.

Callies, J., Corpaccioli, E., Eisinger, M., Hahne, A., and Lefebvre, A.: GOME-2 – MetOp's Second Generation Sensor for Operational Ozone Monitoring, ESA Bulletin, No. 102, 2000.

Chance, K. V. and Spurr, R. J. D.: Ring effect studies: Rayleigh scattering, including molecular parameters for rotational Raman scattering, and the Fraunhofer spectrum, Appl. Opt., 36, 5224–5230, doi:10.1364/AO.36.005224, 1997.

Coburn, S., Dix, B., Sinreich, R., and Volkamer, R.: The CU ground MAX-DOAS instrument: characterization of RMS noise limitations and first measurements near Pensacola, FL of BrO, IO, and CHOCHO, Atmos. Meas. Tech., 4, 2421-2439, doi:10.5194/amt-4-2421-2011, 2011.

Danckaert, T., Fayt, C., Van Roozendael, M., De Smedt, I., Letocart, V., Merlaud, A., and Pinardi, G.: QDOAS Software user manual, Belgian Institute for Space Aeronomy (BIRA-IASB), version 3.2, 2017.

De Smedt, I., Müller, J.-F., Stavrakou, T., Van der A, R., Eskes, H., and Van Roozendael, M.: Twelve years of global observations of formaldehyde in the troposphere using GOME and SCIAMACHY sensors, Atmos. Chem. Phys., 8, 4947–4963, doi:10.5194/acp-8-4947-2008, 2008.

De Smedt, I., Ph.D. Thesis: Long-Term Global Observations of Tropospheric Formaldehyde Retrieved from Spaceborne Nadir UV Sensors, Universite Libre De Bruxelles, Laboratoire de Chimie Quantique et Photophysique, Faculté de Sciences Appliquées, 2011.

De Smedt, I., Van Roozendael, M., Stavrakou, T., Müller, J.-F., Lerot, C., Theys, N., Valks, P., Hao, N., and Van der A, R.: Improved retrieval of global tropospheric formaldehyde columns from GOME-2/MetOp-A addressing noise reduction and instrumental degradation issues, Atmos. Meas. Tech., 5, 2933–2949, doi:10.5194/amt-5-2933-2012, 2012.

De Smedt, I., Stavrakou, T., Hendrick, F., Danckaert, T., Vlemmix, T., Pinardi, G., Theys, N., Lerot, C., Gielen, C., Vigouroux, C., Hermans, C., Fayt, C., Veefkind, P., Müller, J.-F., and Van Roozendael, M.: Diurnal, seasonal and long-term variations of global formaldehyde columns inferred from combined OMI and GOME-2 observations, Atmos. Chem. Phys., 15, 12519–12545, doi:10.5194/acp-15-12519-2015, 2015.

De Smedt, I., Richter, A., Beirle, B., Danckaert, T., Van Roozendael, M., Vlietinck, J., Yu, H., Boesch, T., Hillboll, A., Peters, E., Wagner, T., Wang, Y., Lorente, A., Eskes, H., Van Geffen, J., Zara, M., and Boersma, F.: Tropospheric HCHO retrieved from OMI, GOME (-2), and SCIAMACHY within the Quality Assurance For Essential Climate Variables (QA4ECV) project, EGU General Assembly Conference Abstracts, 2017.

De Smedt, I., Yu, H., Richter, A., Beirle, S., Eskes, H., Boersma, K.F., Van Roozendael, M., Van Geffen, J., Lorente, A. and Peters, E.: QA4ECV HCHO tropospheric column data from OMI (Version 1.1) [Data set]. Royal Belgian Institute for Space Aeronomy, http://doi.org/10.18758/71021031, 2017.

De Smedt, I., Theys, N., Yu, H., Danckaert, T., Lerot, C., Compernolle, S., Van Roozendael, M., Richter, A., Hilboll, A., Peters, E., Pedergnana, M., Loyola, D., Beirle, S., Wagner, T., Eskes, H., van Geffen, J., Boersma, K. F., and Veefkind, P.: Algorithm theoretical baseline for formaldehyde retrievals from S5P TROPOMI and from the QA4ECV project, Atmos. Meas. Tech., 11, 2395-2426, https://doi.org/10.5194/amt-11-2395-2018, 2018.

Dikty, S. and Richter, A.: GOME-2 on MetOp-A Support for Analysis of GOME-2 In-Orbit Degradation and Impacts on Level 2 Data Products, ITT 09/10000262, Final Report, Version 2.0, 2011.

Dirksen, R., Dobber, M., Voors, R., and Levelt, P.: Prelaunch characterization of the Ozone Monitoring Instrument transfer function in the spectral domain, Appl. Opt., 45(17), 3972–3981, doi:10.1364/AO.45.003972, 2006.

Dirksen, R. J., Boersma, K. F., Eskes, H. J., Ionov, D. V., Bucsela, E. J., Levelt, P. F., and Kelder, H. M.: Evaluation of stratospheric NO2 retrieved from the Ozone Monitoring Instrument: Intercomparison, diurnal cycle, and trending, J. Geophys. Res., 116, D08305, doi:10.1029/2010JD014943, 2011.

Dobber, M. R., Dirksen, R. J., Levelt, P. F., van den Oord, G.H.J., Voors, R.H.M., Kleipool, Q., Jaross, G., Kowalewski, M., Hilsenrath, E., Leppelmeier, G.W., de Vries, J., Dierrsen, W., Rozemeijer, N.C.: Ozone Monitoring Instrument calibration, IEEE Trans. Geosci. Remote Sens., 44, 1209, doi:10.1109/TGRS.2006.869987, 2006.

Dobber, M., Kleipool, Q., Dirksen, R., Levelt, P., Jaross, G., Taylor, S., Kelly, T., and Flynn, L.: Validation of ozone monitoring instrument level-1b data products, J. Geophys. Res., 113, D15S06, doi:10.1029/2007JD008665, 2008.

Dufour, G., Szopa, S., Barkley, M. P., Boone, C. D., Perrin, A., Palmer, P. I., and Bernath, P. F.: Global upper-tropospheric formaldehyde: seasonal cycles observed by the ACE-FTS satellite instrument, Atmos. Chem. Phys., 1051-1095, 2009.

EUMETSAT: Investigation on GOME-2 Throughput Degradation, EUMETSAT, Darmstadt, Germany, EUM/LEO/REP/09/0732, Issue 1.1, 58 pp., https://www.eumetsat.int/website/wcm/idc/idcplg?IdcService=GET_FILE&dDocName=PDF_GOME_THRU_DEG_ESA&RevisionSelectionMethod=LatestReleased&Rendition=Web, 2011.

Fischer, P. H., Marra, M., Ameling, C. B., Hoek, G., Beelen, R., de Hoogh, K., ... and Houthuijs, D.: Air pollution and mortality in seven million adults: The Dutch Environmental Longitudinal Study (DUELS). Environmental health perspectives, 123(7), 697, 2015.

GCOS-138: Implementation plan for the Global Observing System for Climate in Support of the UNFCCC (2010 Update), Publication No. GCOS-138, COP-16, 2010.

GCOS-154: Systematic Observation Requirements for Satellite-based Products for Climate Supplemental details to the satellite-based component of the Implementation Plan for the Global Observing System for Climate in Support of the UNFCCC (2011 Update), 2011.

GCOS-200: The Global Observing System for Climate: Implementation Needs, 2016.

González Abad, G., Liu, X., Chance, K., Wang, H., Kurosu, T. P., and Suleiman, R.: Updated Smithsonian Astrophysical Observatory Ozone Monitoring Instrument (SAO OMI) formaldehyde retrieval, Atmos. Meas. Tech., 8, 19-32, https://doi.org/10.5194/amt-8-19-2015, 2015.

Grainger, J. F. and Ring, J.: Anomalous Fraunhofer line profiles, Nature, 193, p. 762, doi:10.1038/193762a0, 1962.

IPCC (2013). Climate Change 2013: The Physical Science Basis. Contribution of Working Group I to the Fifth Assessment Report of the Intergovernmental Panel on Climate Change, T.F. Stocker, D. Qin, G.-K. Plattner, M. Tignor, S.K. Allen, J. Boschung, A. Nauels, Y. Xia, V. Bex, P.M. Midgley (eds.), Cambridge, United Kingdom and New York, NY, USA, 1535 pp, doi:10.1017/CBO9781107415324, 2013.

Joiner, J., Guanter, L., Lindstrot, R., Voigt, M., Vasilkov, A. P., Middleton, E. M., Huemmrich, K. F., Yoshida, Y., and Frankenberg, C.: Global monitoring of terrestrial chlorophyll fluorescence from moderate-spectral-resolution near-infrared satellite measurements: methodology, simulations, and application to GOME-2, Atmos. Meas. Tech., 6, 2803–2823, doi:10.5194/amt- 6-2803-2013, 2013.

Veihelmann, B. and Kleipool, Q.: Reducing Along-Track Stripes in OMI-Level 2 Products, TN-OMIE-KNMI-785, 24 pp., 2006.

Krotkov, N. A., Lamsal, L. N., Celarier, E. A., Swartz, W. H., Marchenko, S. V., Bucsela, E. J., Chan, K. L., Wenig, M., and Zara, M.: The version 3 OMI NO_2 standard product, Atmos. Meas. Tech., 10, 3133-3149, doi.org/10.5194/amt-10-3133-2017, 2017.

Lacan, A. and Lang, R.: Investigation on GOME-2 throughput degradation, Final report, EUM/LEO/REP/09/0732 Issue 1.1, 16 July, 2011.

Lamsal, L. N., Duncan, B. N., Yoshida, Y., Krotkov, N. A., Pickering, K. E., Streets, D. G., and Lu, Z.: U.S. NO2 trends (2005–2013): EPA Air Quality System (AQS) data versus improved observations from the Ozone Monitoring Instrument (OMI), Atmos. Env., 110, pp:130-143, doi:10.1016/j.atmosenv.2015.03.055, 2015.

Leue, C., M. Wenig, T. Wagner, U. Platt, and B. Jähne, Quantitative analysis of NOx emissions from GOME satellite image sequences, J. Geophys. Res.,106, 5493-5505, 2001.

Levelt, P. F., Van den Oord, G. H. J., Dobber, M. R., Mälkki, A., Visser, H., De Vries, J., Stammes, P., Lundell, J. O. V, and Saari, H.: The Ozone Monitoring Instrument, IEEE Transaction on Geoscience and Remote Sensing, 44(5), 1093–1101, 2006b.

Liu, S., Valks P., Pinardi, G., De Smedt, I., Yu, H., and Beirle, S.: An Improved total and tropospheric NO2 column retrieval for GOME-2, Proc. 'Living Planet Symposium 2016', Prague, Czech Republic, 2016.

Lorente, A., Boersma, K. F., Yu, H., Dörner, S., Hilboll, A., Richter, A., Liu, M., Lamsal, L. N., Barkley, M., De Smedt, I., Van Roozendael, M., Wang, Y., Wagner, T., Beirle, S., Lin, J.-T., Krotkov, N., Stammes, P., Wang, P., Eskes, H. J., and Krol, M.: Structural uncertainty in air mass factor calculation for NO2 and HCHO satellite retrievals, Atmos. Meas. Tech., 10, 759-782, doi:10.5194/amt-10-759-2017, 2017.

Marchenko, S., Krotkov, N. A., Lamsal, L. N., Celarier, E. A., Swartz, W. H., and Bucsela, E. J.: Revising the slant column density retrieval of nitrogen dioxide observed by the Ozone Monitoring Instrument, J. Geophys. Res. Atmos., 120, 5670–5692, doi:10.1002/2014JD022913, 2015.

McPeters, R. D., Frith, S., and Labow, G. J.: OMI total column ozone: extending the long-term data record, Atmos. Meas. Tech., 8, 4845-4850, https://doi.org/10.5194/amt-8-4845-2015, 2015.

Mijling, B., Van der A, R. J., Boersma, K. F., Van Roozendael, M., De Smedt, I., and Kelder, H. M.: Reductions of NO2 detected from space during the 2008 Beijing Olympic Games, Geophysical Research Letters, Vol. 36, L13801, doi:10.1029/2009GL038943, 2009.

Millet, D. B., Jacob, D. J., Boersma, K. F., Fu, T.-M., Kurosu, T. P., Chance, K., Heald, C. L., and Guenther, A.: Spatial distribution of isoprene emissions from North America derived from formaldehyde column measurements by the OMI satellite sensor, J Geophys. Res. 113 (2008), p. D02307, doi:10.1029/2007JD008950, 2008.

Miyazaki, K., Eskes, H., Sudo, K., Boersma, K. F., Bowman, K., and Kanaya, Y.: Decadal changes in global surface NOx emissions from multi-constituent satellite data assimilation, Atmos. Chem. Phys., 17, 807-837, doi:10.5194/acp-17-807-2017, 2017.

Müller, J.-P., Kharbouche, S., Gobron, N., Scanlon, T., Govaerts, Y., Danne, O., Schultz, J., Lattanzio, A., Peters, E., De Smedt, I., Beirle, S., Lorente, A., Coheur, P. F., George, M., Wagner, T., Hilboll, A., Richter, A., Van Roozendael, M., and Boersma, K. F.: Recommendations (scientific) on best practices for retrievals for Land and Atmosphere ECVs (QA4ECV Deliverable 4.2 version 1.0), 186 pp., http://www.qa4ecv.eu/sites/default/files/D4.2.pdf, last access: 12 April 2018, 2016.

Munro, R., Lang, R., Klaes, D., Poli, G., Retscher, C., Lindstrot, R., Huckle, R., Lacan, A., Grzegorski, M., Holdak, A., Kokhanovsky, A., Livschitz, J., and Eisinger, M.: The GOME-2 instrument on the Metop series of satellites: instrument design, calibration, and level 1 data processing – an overview, Atmos. Meas. Tech., 9, 1279–1301, doi:10.5194/amt-9-1279-2016, 2016.

Pommereau, J.-P. and Goutail, F.: O3 and NO2 ground-based measurements by visible spectrometry during arctic winter and spring 1988, Geophys. Res. Lett., 15, 891–894, 1988.

Peters, E., Wittrock, F., Richter, A., Alvarado, L. M. A., Rozanov, V. V., and Burrows, J. P.: Liquid water absorption and scattering effects in DOAS retrievals over oceans, Atmos. Meas. Tech., 7, 4203–4221, doi:10.5194/amt-7-4203-2014, 2014.

Puķīte, J., Kühl, S., Deutschmann, T., Platt, U., and Wagner, T.: Extending differential optical absorption spectroscopy for limb measurements in the UV, Atmos. Meas. Tech., 3, 631-653, https://doi.org/10.5194/amt-3-631-2010, 2010.

Platt, U.: Air Monitoring by Differential Optical Absorption Spectroscopy. Encyclopedia of Analytical Chemistry. 1–28, 2017.

Press, W. H., Teukolsky, S. A., Vetterling, W. T., and Flannery, B. P.: Numerical recipes in Fortran 77: The art of scientific computing, Second edition, Vol. 1 of Fortran Numerical Recipes, 1997.

~~QA4ECV: WP4: Recommendations on best practices for Land and Atmosphere ECVs (Section 2.3 - Spectral Fitting Best Practices and Recommendations), Deliverable 4.2, 2016.~~

Richter, A.: Absorptionsspektroskopische Messungen stratosphärischer Spurengase über Bremen, 53° N., PhD-Thesis, University of Bremen, 1997.

Richter, A., Begoin, M., Hilboll, A., and Burrows, J. P.: An improved NO2 retrieval for the GOME-2 satellite instrument, Atmos. Meas. Tech., 4(6), 1147–1159, doi:10.5194/amt-4-1147-2011, 2011.

Richter, A., Wittrock F., and Burrows, J.P.: Development of an OClO Slant Column Product for the GOME-2 Sensors, EGU General Assembly, Vienna, Austria, 2016.

Sanders, A. F., Verstraeten, W. W., Kooreman, M. L., Van Leth, T. C., Beringer, J., and Joiner, J.: Spaceborne Sun-Induced Vegetation Fluorescence Time Series from 2007 to 2015 Evaluated with Australian Flux Tower Measurements. Remote Sensing, 8(11), 895, 2016.

~~S5P/TROPOMI HCHO ATBD, S5P-BIRA-L2-400F-ATBD, CI-400F-ATBD, Issue: 1.0.0, 2016.~~

Schenkeveld, E.V.M., Jaross, G., Marchenko, S., Haffner, D., Kleipool, Q.L., Rozemeijer, N.C., Veefkind, P.J., Levelt, P.F.: In-flight performance of the Ozone Monitoring Instrument, Atmos. Meas. Tech., 10, 1957-1986, doi:10.5194/amt-10-1957-2017, 2017.

Sillman, S., Logan, J. A., and Wofsy, S. C.: The sensitivity of ozone to nitrogen oxides and hydrocarbons in regional ozone episodes, J. Geophys. Res., 95(D2), 1837–1851, doi:10.1029/JD095iD02p01837, 1990.

Spurr, R.: LIDORT and VLIDORT: Linearized pseudo-spherical scalar and vector discrete ordinate radiative transfer models for use in remote sensing retrieval problems. Light Scattering Reviews, 3, ed. A. Kokhanovsky, Springer, 2008.

Sun, K., Liu, X., Huang, G., González Abad, G., Cai, Z., Chance, K., and Yang, K.: Deriving the slit functions from OMI solar observations and its implications for ozone-profile retrieval, Atmos. Meas. Tech. Discuss., https://doi.org/10.5194/amt-2017-129, in review, 2017.

Valks, P., Pinardi, G., Richter, A., Lambert, J.-C., Hao, N., Loyola, D., Van Roozendael, M., and Emmadi, S.: Operational total and tropospheric NO2 column retrieval for GOME-2, Atmos. Meas. Tech., 4, 1491–1514, doi:10.5194/amt-4-1491-011, 2011.

Van Geffen, J. H. G. M., Boersma, K. F., Van Roozendael, M., Hendrick, F., Mahieu, E., De Smedt, I., Sneep, M., and Veefkind, J. P.: Improved spectral fitting of nitrogen dioxide from OMI in the 405–465 nm window, Atmos. Meas. Tech., 8, 1685–1699, doi:10.5194/amt-8-1685-2015, 2015.

Verstraeten, W. W., Neu, J. L., Williams, J. E., Bowman, K. W., Worden, J. R., and Boersma, K. F.: Rapid increases in tropospheric ozone production and export from China, Nature Geoscience, 8, 690–695, doi:10.1038/ngeo2493, 2015.

Voors, R., Dobber, M., Dirksen, R., and Levelt, P.: Method of calibration to correct for cloud-induced wavelength shifts in the Aura satellite's Ozone Monitoring Instrument, Applied optics, 45, 3652–3658, 2006.

Vountas, M., Rozanov, V., and Burrows, J.: Ring effect: Impact of rotational Raman scattering on radiative transfer in Earth's atmosphere, J. Quant. Spectrosc. Ra., 60, 943–961, doi:10.1016/S0022-4073(97)00186-6, 1998.

Wenig, M., Ph.D. Thesis: Satellite Measurement of Long-Term Global Tropospheric Trace Gas Distributions and Source Strengths - Algorithm Development and Data Analysis, part of the German Research Foundation (DFG) research unit "Image Sequence Analysis to Investigate Dynamic Processes", 2001.

Zhu, L., Jacob, D. J., Keutsch, F. N., Mickley, L. J., Scheffe, R., Strum, M., González Abad, G. et al.: Formaldehyde (HCHO) As a Hazardous Air Pollutant: Mapping Surface Air Concentrations from Satellite and Inferring Cancer Risks in the United States, Environmental Science & Technology 51, no. 10 (2017): 5650-5657, 2017.

Supplement of

Improved slant column density retrieval of nitrogen dioxide and formaldehyde for OMI and GOME-2A from QA4ECV: intercomparison, uncertainty characterization, and trends

Marina Zara et al.

Correspondence to: Marina Zara (marina.zara@knmi.nl)

Disentanglement scheme to investigate NO_2 SCD uncertainty dependencies

The statistical NO_2 SCD uncertainty decreases with increasing SCD, most notably for OMNO2-NASA. To further investigate whether SCD uncertainty reduction is driven by the SCD itself ("more signal") or by the top-of-atmosphere reflectance levels ("better signal-to-noise"), we use a 3-step disentanglement scheme wherein our ensemble of Pacific observations 1) are divided in AMF bins, 2) each AMF-bin is divided into SCD sub-bins, and 3) each SCD sub-bin is sliced in low top-of-atmosphere reflectance ($R < 0.04$) and high top-of-atmosphere reflectance ($R > 0.2$) boxes. Hereby we can analyze whether SCD uncertainties for low reflectance and high reflectance scenes are significantly different for pixels with very similar AMFs and SCDs.

The distribution of the deviations of the SCDs from the box-mean SCD for the low-reflectance and the high-reflectance scenes with similar AMF and SCD values for OMINO2-QA4ECV is shown in Figure S1. The box-mean AMFs and SCDs used here were 2.25±0.25 and $5\pm1\times10^{15}$ molec. cm^{-2}, respectively.

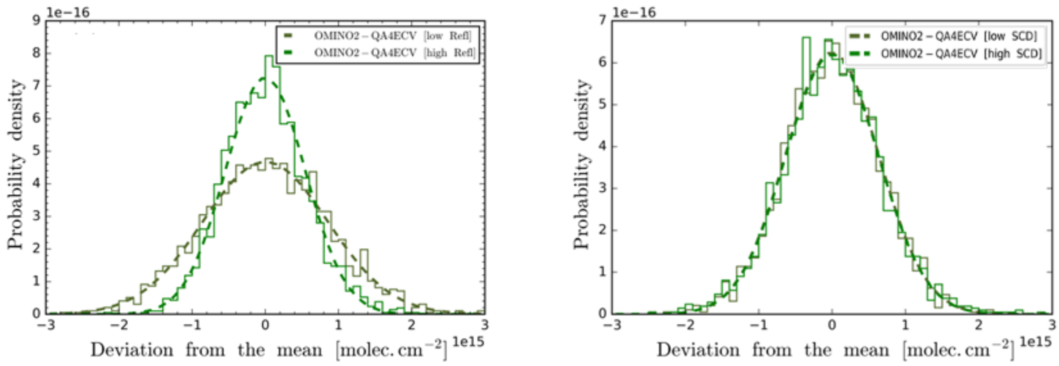

Figure S1. Distribution of the deviation of the OMI NO_2 SCDs from the mean-SCD within [left] low-reflectance (dark-green line) and high-reflectance (light-green line) boxes, and [right] low-SCD (dark-green line) and high-SCD (light-green line) within the same sub-bin in a histogram for OMINO2-QA4ECV.

The NO_2 SCD uncertainties are substantially higher for low-reflectance than for high-reflectance scenes (Table S1). Over bright scenes, the OMINO2-QA4ECV SCD uncertainty is 35% lower than for dark scenes. This suggests that the top-of-atmosphere reflectance is potentially the main SCD-uncertainty driver.

Table S1. Statistical uncertainty estimates of OMI NO_2 SCDs for the OMINO2-QA4ECV algorithm for boxes within the same AMF-bin; boxes in the same SCD sub-bin are divided in low- and high- reflectance boxes (left), and boxes in the same reflectance sub-bin are divided in low- and high- SCD boxes (right).

	OMINO2-QA4ECV SCD uncertainty [molec. cm^{-2}]	[molec. cm^{-2}]	OMINO2-QA4ECV SCD uncertainty [molec. cm^{-2}]
Low-Refl. (<0.04)	0.86×10^{15}	Low-SCD ($<7\times10^{15}$)	0.64×10^{15}
High-Refl. (>0.2)	0.55×10^{15}	High-SCD ($>12\times10^{15}$)	0.64×10^{15}

We repeat the same procedure to investigate whether SCD uncertainties for low and high SCD values are significantly different for pixels with very similar AMFs and top-of-atmosphere reflectance levels. We create AMF bins and reflectance sub-bins, with low-SCD ($SCD < 7\times10^{15}$ molec. cm^{-2}) and high-SCD ($SCD > 12\times10^{15}$ molec. cm^{-2}) boxes. The box-mean AMFs and reflectances were 3.75±0.25 and 0.1±0.02, respectively. We see that for OMINO2-QA4ECV the NO_2 SCD uncertainty has the same value for both low- and high- SCD boxes (Table S1), indicating that the SCD uncertainty does not depend on the SCD value. The OMNO2A v2 algorithm (not shown) yields similar results to OMINO2-QA4ECV for both schemes. OMNO2-NASA uncertainties differ for the low- and high-SCD indicating that they are more sensitive to SCD values (Figure 7a).

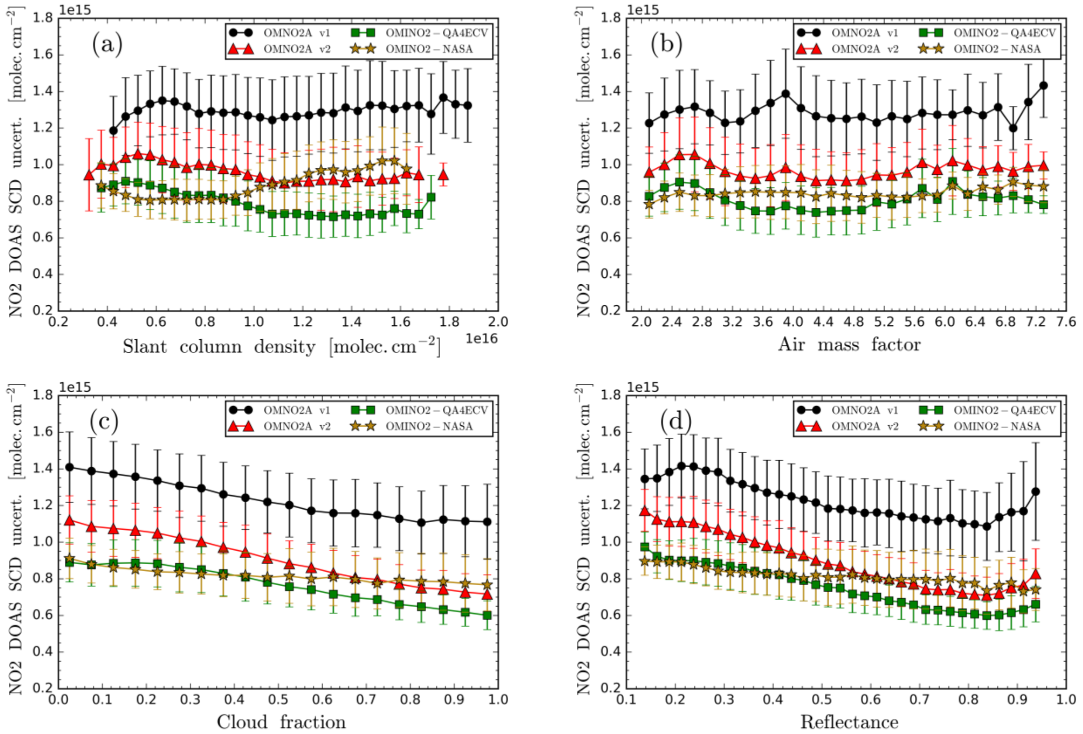

Figure S2. The DOAS OMI NO_2 SCD uncertainty as a function of the (a) SCD, (b) AMF, (c) cloud fraction, and (d) the top-of-atmosphere reflectance for OMNO2A v1 (black circles), OMNO2A v2 (red triangles), OMINO2-QA4ECV (green squares) and OMNO2-NASA (yellow stars) SCDs for the Pacific orbit from day 1 of January, April, July and October (or closest available data) 2005-2015. Each bin contains at least 10 boxes for robust statistics and intercomparisons. The error bars represent one standard deviation (1σ).

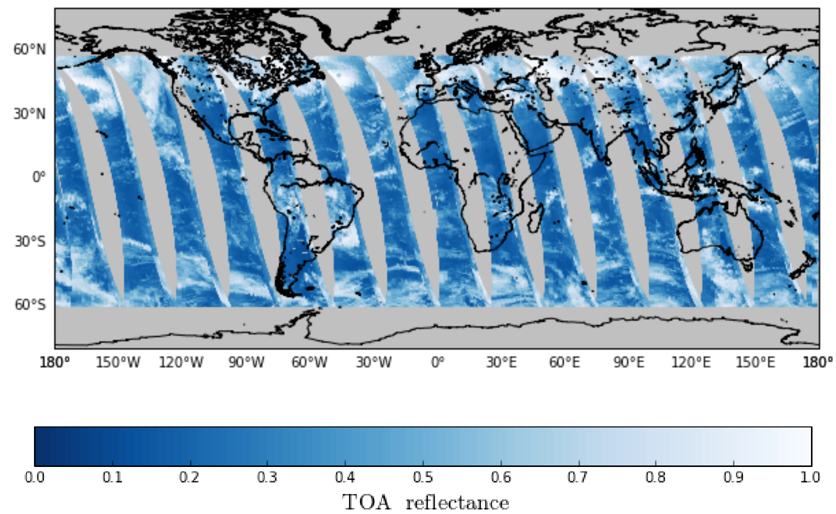

Figure S3. ~~NO$_2$ SCD (top panel) from OMINO2-QA4ECV and t~~Top-of-atmosphere reflectance ~~(bottom panel)~~ on 1 January 2012.

Note: The NO_2 SCD map is now removed.

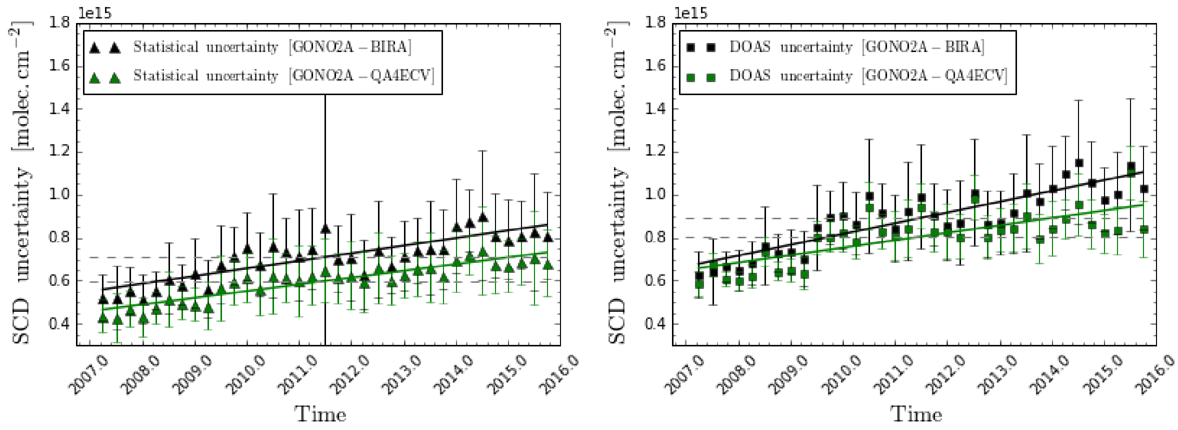

Figure S4. Temporal evolution of the statistical (triangles) and DOAS (squares) GOME-2A NO_2 SCD uncertainty over 2007-2015 (Pacific orbit from day 1 of January, April, August, October- or closest available data) for GONO2A-BIRA (black), and GONO2A-QA4ECV (green) algorithms. Error bars represent one standard deviation (1σ). Solid lines represent the linear regressions fitted to the data for the 9-year period. The slope, *p*, of each fit on the statistical, p^s, and DOAS uncertainty, p^d, is:

$p^{\mathrm{s}}_{\mathrm{bira}} = 0.035 \times 10^{15} \pm 0.004 \times 10^{15}$ molec. cm^{-2} yr^{-1} and $p^{\mathrm{d}}_{\mathrm{bira}} = 0.050 \times 10^{15} \pm 0.005 \times 10^{15}$ molec. cm^{-2} yr^{-1},

$p^{\mathrm{s}}_{\mathrm{qa4ecv}} = 0.031 \times 10^{15} \pm 0.002 \times 10^{15}$ molec. cm^{-2} yr^{-1} and $p^{\mathrm{d}}_{\mathrm{qa4ecv}} = 0.035 \times 10^{15} \pm 0.006 \times 10^{15}$ molec. cm^{-2} yr^{-1}.

Table S2. Yearly increase of the statistical and DOAS uncertainty estimates of GOME-2A NO_2 SCDs for GONO2A-BIRA and GONO2A-QA4ECV algorithms for the Pacific orbit from day 1 of January, April, July and October 2007-2015 for all-sky conditions (top panel) and clear-sky conditions (cloud radiance fraction < 0.5) (bottom panel).

SCD uncertainty (all-sky)	GONO2A-BIRA (2007-2015) [yr^{-1}]	GONO2A-QA4ECV (2007-2015) [yr^{-1}]	SCD uncertainty (crf < 0.5)	GONO2A-BIRA (2007-2015) [yr^{-1}]	GONO2A-QA4ECV (2007-2015) [yr^{-1}]
Statistical	6.3%	6.7%		7.2%	6.9%
DOAS	7.4%	5.3%		7.8%	6.8%

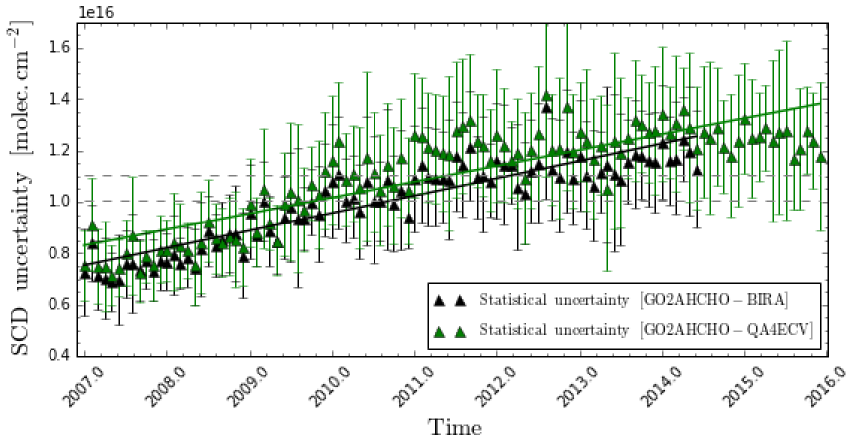

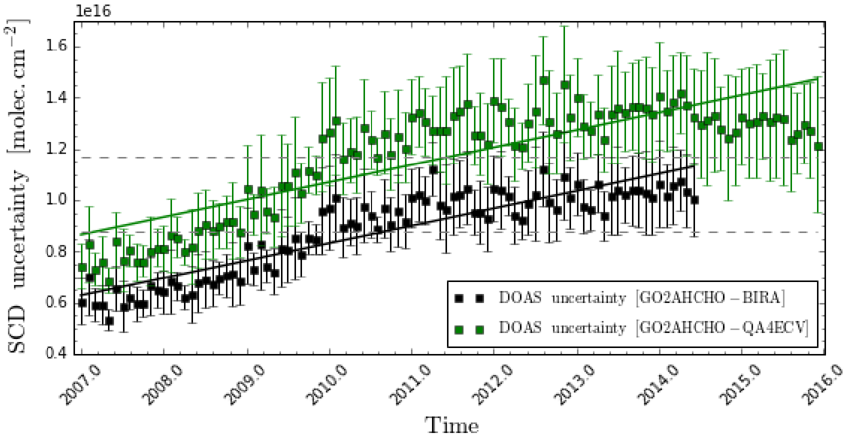

Figure S5. Temporal evolution of the statistical (triangles) and DOAS (squares) GOME-2A HCHO SCD uncertainty over 2007-2015 for GO2AHCHO-BIRA (black) and GO2AHCHO-QA4ECV (green) (Pacific orbit from day 1 of January up to December and from day 15 of January, April, July and October 2007-June 2014 and 2007-2015, respectively). Error bars represent one standard deviation (1σ). Solid lines represent the linear regressions fitted to the data for each period (Table S3). The slope, *p*, of each fit on the statistical, p^s, and DOAS uncertainty, p^d, for GO2AHCHO is:

$p^{s}_{\mathrm{bira}} = 0.68 \times 10^{15} \pm 0.03 \times 10^{15}$ molec. cm^{-2} yr^{-1} and $p^{d}_{\mathrm{bira}} = 0.68 \times 10^{15} \pm 0.04 \times 10^{15}$ molec. cm^{-2} yr^{-1},

$p^{s}_{\mathrm{qa4ecv}} = 0.62 \times 10^{15} \pm 0.04 \times 10^{15}$ molec. cm^{-2} yr^{-1} and $p^{d}_{\mathrm{qa4ecv}} = 0.68 \times 10^{15} \pm 0.04 \times 10^{15}$ molec. cm^{-2} yr^{-1}.

Table S3. Yearly increase of the statistical and DOAS uncertainty estimates of GOME-2A HCHO SCDs for GO2AHCHO-BIRA and GO2AHCHO-QA4ECV (Pacific orbit from day 1 of January up to December and from day 15 of January, April, July and October 2007-June 2014 and 2007-2015, respectively) for all-sky conditions (top panel) and clear-sky conditions (bottom panel). The GO2AHCHO-BIRA data are provided only for scenes with cloud fraction lower than 0.4, therefore the clear-sky conditions yield similar SCD uncertainties to the all-sky conditions.

SCD uncertainty (all-sky)	GO2AHCHO-BIRA (2007-2014) [yr^{-1}]	GO2AHCHO-QA4ECV (2007-2015) [yr^{-1}]	SCD uncertainty (crf < 0.5)	GO2AHCHO-BIRA (2007-2014) [yr^{-1}]	GO2AHCHO-QA4ECV (2007-2015) [yr^{-1}]
Statistical	9.0%	7.4%		10.3%	9.3%
DOAS	10.8%	7.8%		10.8%	9.2%

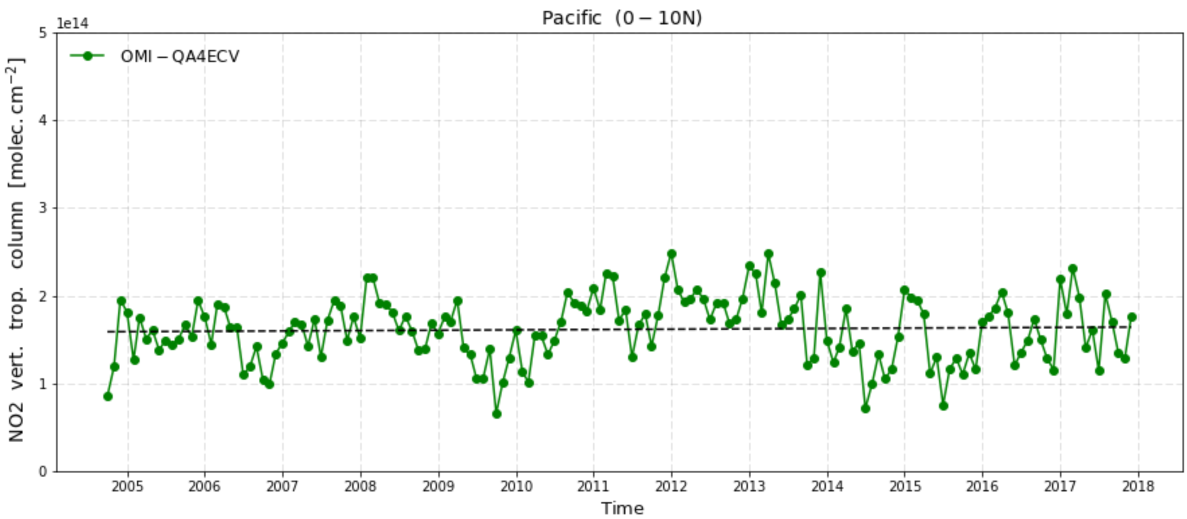

Figure S6: Temporal evolution of monthly means of OMI NO_2 vertical tropospheric columns from QA4ECV over the Pacific [0-10°N] for the 2004-2017 period. The black dashed line is linear regression fitted through the data.

Figure S6 shows the evolution of the QA4ECV OMI NO_2 tropospheric columns over the Pacific [0-10°N] in time [2004-2017]. There is no apparent trend in the NO_2 tropospheric columns, as expected for such a pristine region. The same holds for GOME-2A (not shown). We conclude that in this region, where AMF uncertainties are negligible, any contributions from uncertainties from spectral fitting and stratospheric correction are very small and are indicative for a decadal trend uncertainty from these terms of less than 0.1×10^{15} molec. cm^{-2} dec^{-1}. Over other, polluted, regions, with high AMF uncertainties, the uncertainty in the trends (stability) may well be larger.